iScience

CellPress
OPEN ACCESS

Article

Multilayer and MATR3-dependent regulation of mRNAs maintains pluripotency in human induced pluripotent stem cells

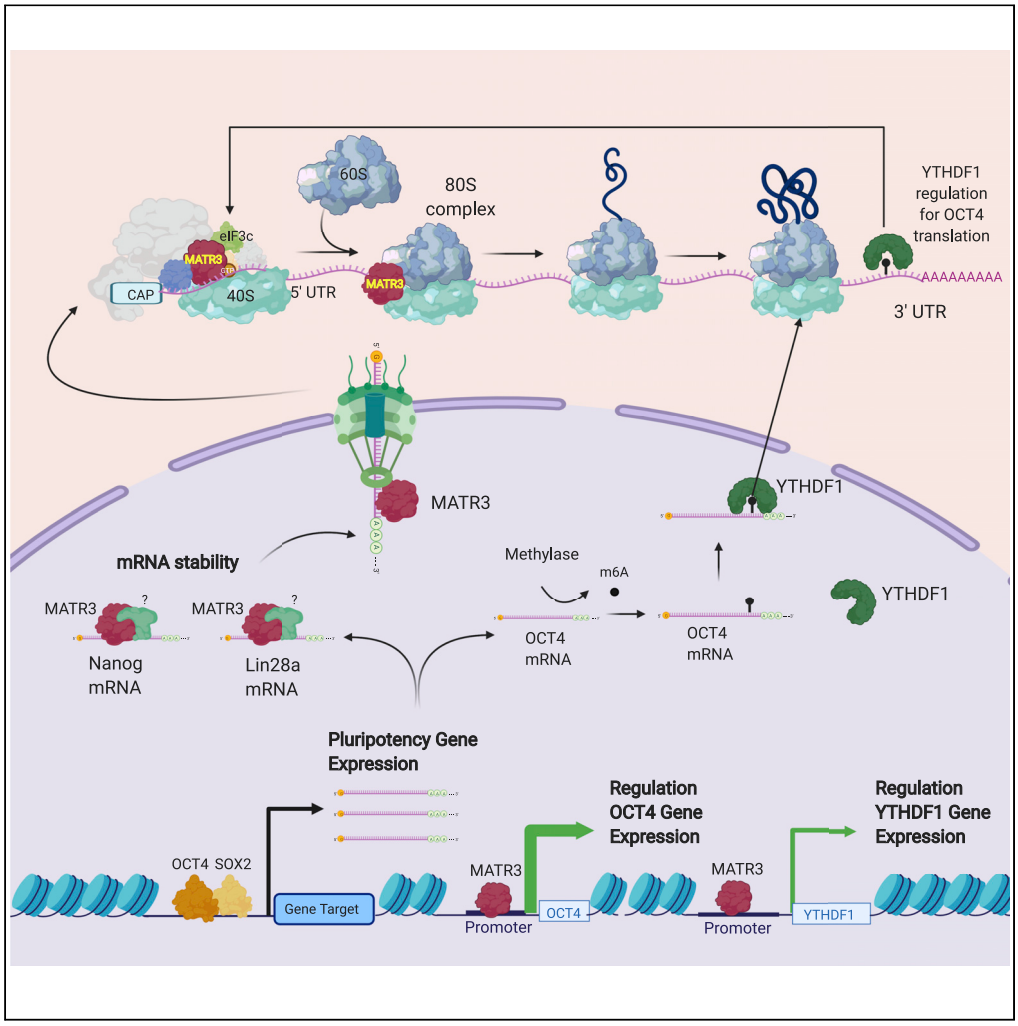

Daniele Pollini, Rosa Loffredo, Federica Maniscalco, ..., Angelo Poletti, Luciano Conti, Alessandro Provenzani

alessandro.provenzani@unitn.it

HIGHLIGHTS

MATR3 orchestrates the pluripotency circuitry in hiPSCs

MATR3 binds to the *OCT4* and *YTHDF1* promoters and favors their expression

YTHDF1 binds the m6A-modified OCT4 mRNA

MATR3 regulates the translation of specific transcripts including NANOG and LIN28A

Pollini et al., iScience *24*, 102197
March 19, 2021
https://doi.org/10.1016/j.isci.2021.102197

iScience

CellPress
OPEN ACCESS

Article

Multilayer and MATR3-dependent regulation of mRNAs maintains pluripotency in human induced pluripotent stem cells

Daniele Pollini,[1] Rosa Loffredo,[1] Federica Maniscalco,[1,5] Marina Cardano,[2] Mariachiara Micaelli,[1] Isabelle Bonomo,[1] Nausicaa Valentina Licata,[1] Daniele Peroni,[3] Weronika Tomaszewska,[1] Annalisa Rossi,[1] Valeria Crippa,[4] Erik Dassi,[1] Gabriella Viero,[5] Alessandro Quattrone,[1] Angelo Poletti,[4] Luciano Conti,[1] and Alessandro Provenzani[1,*]

SUMMARY

Matrin3 (MATR3) is a nuclear RNA/DNA-binding protein that plays pleiotropic roles in gene expression regulation by directly stabilizing target RNAs and supporting the activity of transcription factors by modulating chromatin architecture. MATR3 is involved in the differentiation of neural cells, and, here, we elucidate its critical functions in regulating pluripotent circuits in human induced pluripotent stem cells (hiPSCs). MATR3 downregulation affects hiPSCs' differentiation potential by altering key pluripotency regulators' expression levels, including OCT4, NANOG, and LIN28A by pleiotropic mechanisms. MATR3 binds to the *OCT4* and *YTHDF1* promoters favoring their expression. YTHDF1, in turn, binds the m6A-modified OCT4 mRNA. Furthermore, MATR3 is recruited on ribosomes and controls pluripotency regulating the translation of specific transcripts, including NANOG and LIN28A, by direct binding and favoring their stabilization. These results show that MATR3 orchestrates the pluripotency circuitry by regulating the transcription, translational efficiency, and epitranscriptome of specific transcripts.

INTRODUCTION

MATR3 is a highly conserved 125-kDa protein, abundantly expressed in the inner nuclear matrix (Zeitz et al., 2009). It has a multi-domain structure composed of a nuclear localization signal (NLS), two C2H2-type zinc finger DNA-binding domains, and two RNA recognition motif domains (Belgraders et al., 1991; Hisada-Ishii et al., 2007). MATR3 plays pleiotropic roles by binding both DNA and RNA, and it is involved in RNA metabolism, regulating the levels of long noncoding RNAs (Banerjee et al., 2017) and controlling nuclear mRNA export (Boehringer et al., 2017; Zhang and Carmichael, 2001) and mRNA stabilization (Salton et al., 2011). RNA-mediated MATR3 interaction with DHX9 and HNRNPK indicates that MATR3 is involved in the assembly of multiprotein complexes to exert its functions in RNA metabolism (Salton et al., 2011). MATR3 was initially identified as a nuclear scaffold protein involved in the assembly of the internal fibrogranular network by binding DNA sites known as matrix/scaffold attachment regions (Hisada-Ishii et al., 2007). The binding of the POU-homeodomain transcription factor Pit1 (Pou1f1) to its transcriptional enhancers is dependent on the presence of a MATR3-rich network: MATR3-dependent physical organization of the chromatin allows the transcriptional assembly of the Pit1-β-catenin-SatB1 complex (Skowronska-Krawczyk et al., 2014). MATR3 genetic variants are associated with autosomal dominant distal myopathy, pharyngeal and vocal cord dysfunction, as well as familial and sporadic cases of amyotrophic lateral sclerosis (ALS) (Johnson et al., 2014; Leblond et al., 2016; Lin et al., 2015; Marangi et al., 2017; Origone et al., 2015). MATR3 has also been found in neuronal cytoplasmic inclusions alone or associated with TDP-43 (Tada et al., 2018), C9orf72 hexanucleotide repeat expansion Di-Peptide Repeats (Johnson et al., 2014), or ectopic ALS-linked FUS mutant (Yamaguchi and Takanashi, 2016) in cells derived from patients with ALS. MATR3 is a key element for neural stem cell (NSC) differentiation, and its role is regulated by ATM-mediated phosphorylation (Niimori-kita et al., 2018), but, to date, its role in pluripotency maintenance and cell fate commitment has not been elucidated. Pluripotent stem cell maintenance and differentiation involves numerous and coordinated changes that require transcription factors, including OCT4, NANOG, SOX2,

[1]Department of Cellular, Computational and Integrative Biology, University of Trento, Trento, Italy

[2]Cell Technology Core Facility, Department of Cellular, Computational and Integrative Biology, University of Trento, Trento, Italy

[3]Mass Spectrometry Core Facility, Department of Cellular, Computational and Integrative Biology, University of Trento, Trento, Italy

[4]Laboratorio di Biologia Applicata, Dipartimento di Scienze Farmacologiche e Biomolecolari, Università degli Studi di Milano, Milan, Italy

[5]Institute of Biophysics, CNR, Trento, Italy

*Correspondence: alessandro.provenzani@unitn.it

https://doi.org/10.1016/j.isci.2021.102197

KLF4 (Takahashi and Yamanaka, 2016), as well as several RNA-binding proteins (RBPs) (Guallar and Wang, 2014). Among the RBPs, the most notable example is LIN28A, a factor that can be used to reprogram human somatic cells to pluripotent stem cells (Yu et al., 2007). The main function of LIN28A is to regulate mRNAs involved in embryonic development by interacting directly with RNAs, such as *OCT4* (Qiu et al., 2009), also in collaboration with other RBPs such as L1TD1 (Närvä et al., 2012), and by disrupting the maturation of certain miRNAs, as the LET7 family (Qiu et al., 2009; Rybak et al., 2008). Other notable examples of RBPs are PTBP1, which is essential for embryonic stem cells (ESC) proliferation (Shibayama et al., 2009), and, more recently, the readers of the N^6-methyladenosine (m6A) RNA modification (Deng et al., 2018), including the YTH domain-containing proteins and the IGF2BP proteins, which bind and regulate the stability or translation of target genes (Huang et al., 2018; Wu et al., 2019). Indeed, transcripts encoding core pluripotency transcription factors are m6A methylated and the decrease of the global RNA methylation status reduces the ESCs' ability to properly differentiate (Batista et al., 2014; Geula et al., 2015). Therefore, the m6A modification plays pivotal physiological functions in regulating RNA metabolism in pluripotency, leading to changes in the expression of key factors such as *OCT4, SOX2, LIN28A,* and *NANOG* (Chen et al., 2015a).

We investigated the role of MATR3 in maintaining pluripotency and generated human iPSCs in which MATR3 was stably silenced. We found that MATR3 plays a critical role in regulating the hiPSCs' single-cell growth, colony formation, and neural differentiation potential, by modulating the expression level of critical regulators of pluripotency including NANOG, LIN28A, and OCT4. MATR3 interactome investigation revealed the role of the protein in the translation process, supported by direct binding and stabilization of NANOG and LIN28A transcripts and thus favoring their expression. In addition, MATR3 chromatin immunoprecipitation (ChIP) revealed a dual level of *OCT4* regulation. MATR3 binds the promoter regions of *OCT4* and *YTHDF1* and regulates their transcription. YTHDF1, an m6A reader, binds and regulates the levels of the m6A OCT4 and LIN28A transcripts. In conclusion, MATR3 contributes, both directly and indirectly, to the maintenance of the pluripotency in hiPSCs, fine-tuning the expression of key pluripotency regulators.

RESULTS

MATR3 is essential for the clonogenic ability of human iPSCs

To understand the role of MATR3 in pluripotency maintenance and differentiation, we generated hiPSCs in which MATR3 was stably silenced by short hairpin RNA (shRNA) strategy. Commercial hiPSCs were infected with lentiviral particles loaded with shRNA sequence targeting human *MATR3* (shMATR3), and stably silenced cells were selected. In the polyclonal shMATR3-iPSC population, MATR3 protein levels were reduced by 60% when compared with control hiPSCs (shCtrl) (Figures 1A, 1B, and S1A). We obtained a homogeneous population in which 55% of the cells showed a decrease of MATR3 (Figures S1A and S1B). shCtrl and shMATR3 cells formed round and compact colonies with no appreciable morphological differences (Figure 1C) and did not show any cell proliferation or viability defects (Figures 1D and 1E). Interestingly, shMATR3 cells exhibited a significant growth deficit in sub-optimal conditions, i.e., following single-cell dissociation. Indeed, shMATR3 cells plated in these conditions showed reduced growth and colony formation ability compared with shCtrl cells (Figures 1F and S1C). The same result was obtained by a limiting dilution assay. Control cells showed no defect in clonogenic capability, whereas only cells with at least 50% of *MATR3* expression level were able to form colonies. In addition, the level of pluripotency markers decreased in accordance with the *MATR3* level (Figures S1D and S1E). These results suggest that MATR3 downregulation does not impact cell growth in standard culturing conditions, but it hampers single-cell growth and colony formation of hiPSCs.

MATR3 is required for hiPSCs neuronal differentiation

As MATR3 downregulation impacts hiPSCs self-renewal, we explored the possible occurrence of defects during the trilineage commitment of shMATR3 cells by performing an embryoid bodies (EBs) assay (Lin et al., 2014) (Figures 2A and S2A). MATR3 silencing impaired EB formation ability of hiPSCS, as shown by the substantial reduction in EB number (Day 7, 47% reduction; Figure 2B) and by the marked, altered morphology of surviving floating EBs (Figure 2A), as shown by an increased elongation distortion index (EDI) (Figure 2C). Following the plating in adhesion and culturing for one additional week, EBs spontaneously differentiated toward cell types representative of all the three germ layers (Figure 2D). Fourteen-day-old MATR3-silenced cultures showed the expression of all three lineage markers and an up-regulation of mRNA expression levels of neuroectodermal (*TUBB3* and *NESTIN*) (Niimori-kita et al., 2018) and

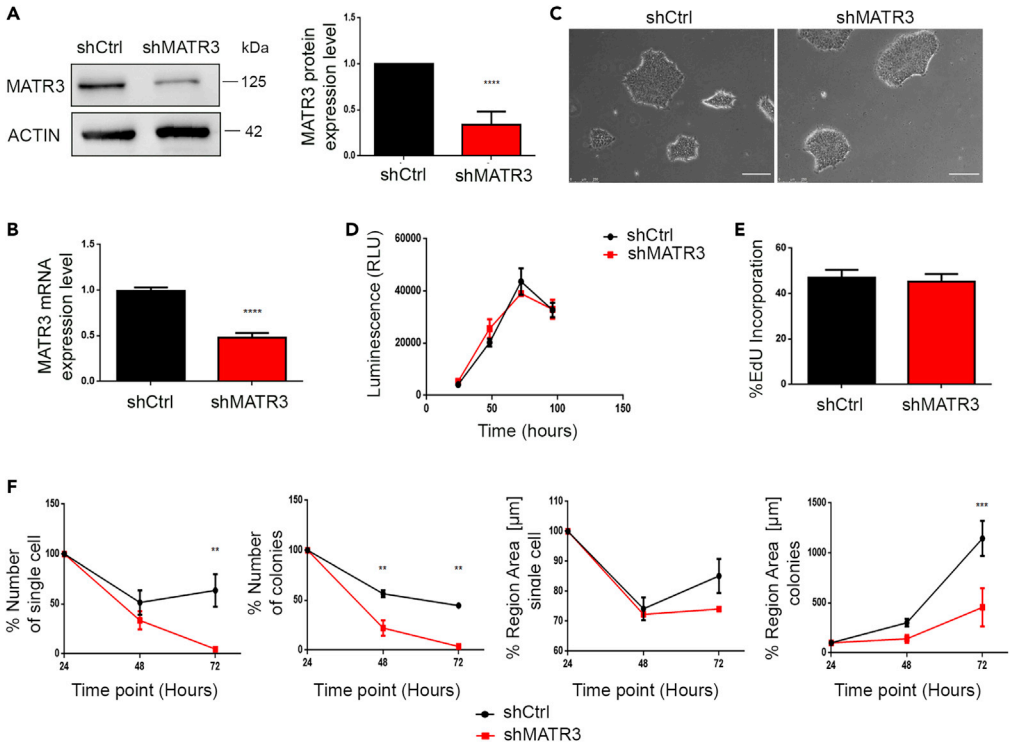

Figure 1. MATR3 is essential for single-cell growth of hiPSCs

(A) MATR3 protein expression levels were analyzed by western blot (WB) in hiPSCs stably infected with shMATR3 and shCtrl lentiparticles. β-ACTIN was used as housekeeping (left panel). MATR3 levels were quantified by densitometry analysis. The bar plots show the mean values of three independent experiments (right panel). Graph represents a mean of three biological replicates ± SEM. p value was calculated by *t* test (****p < 0.0001).

(B) *MATR3* RNA expression levels were measured by real-time qPCR in hiPSC line stably infected with shMATR3 and shCtrl lentiparticles. Data are presented as mean of three biological replicates ± SEM. p value was calculated by *t* test (****p < 0.0001).

(C) Pictures of shCtrl and shMATR3 hiPSCs (scale bar, 250 µm).

(D) Growth curve of shCtrl and shMATR3 hiPSCs were performed using OZBlue assay. Data are presented as the mean ± SEM of three biological replicates; two-way ANOVA (not significant, p>0.05).

(E) EdU proliferation assay for shMATR3 and shCtrl hiPSCs. Percentage of EdU-incorporating cells was measured by flow cytometry. Data are presented as means ± SEM (n = 2 biological replicates, 6 technical replicates); *t* test not significant, p>0.05 .

(F) Analyses of shMATR3 and shCtrl hiPSCs following single-cell seeding. Cells were incubated with AP Live Stain at each time point (time point, 24, 48, and 72 h). Images were acquired with the Operetta High Content Screening System using 2× objective 0.08NA. The region areas [µm] for the single cells and for the colonies are reported for each time point. The comparison is between shCtrl and shMATR3 cells. Two-way ANOVA (** p<0.01; *** p< 0.001).

endodermal (*GATA4*) markers (Vallier et al., 2009). Notably, no alteration in mesodermal marker (*αSMA*) expression was detected (Figure 2E). To better elucidate MATR3 role during *in vitro* neuralization, we exposed shMATR3 (and shCtrl) hiPSCs to monolayer neural induction conditions to generate neural precursors cells (NPCs) (Jha et al., 2015). At Day 12 of the neuralization protocol, cultures were enriched in NPCs as assessed by FABP7 live imaging assay (Leong et al., 2013; Yun et al., 2012) (Figure S2B). NPCs were organized in the neural rosette, i.e., radially ordered structures in which NPCs show apical tight junction marker ZO-1 in the central lumen (Curchoe et al., 2012) (Figure 2F). Quantitative analysis of rosette formation capacity on neural-oriented cultures revealed that shMATR cells had a 2-fold increased capability to generate ZO-1-positive neural rosettes in culture with respect to control cells (Figures 2F and 2G). Moreover, morphometric analyses showed that shMATR3 cultures were characterized by a 2-fold increase in the percentage of rosettes characterized by a small lumen (<101 μm^2) and by a 1.5-fold decrement of medium (101 < area <350 μm^2) and 3-fold decrement of large (>350 μm^2) rosettes (Figure 2G). Differentiation of NPC cultures toward the neuronal lineage showed that shMATR3 cells were characterized by a reduction of neurite length and arborization (Figure S2C). Collectively, these data suggest that MATR3 plays a pivotal

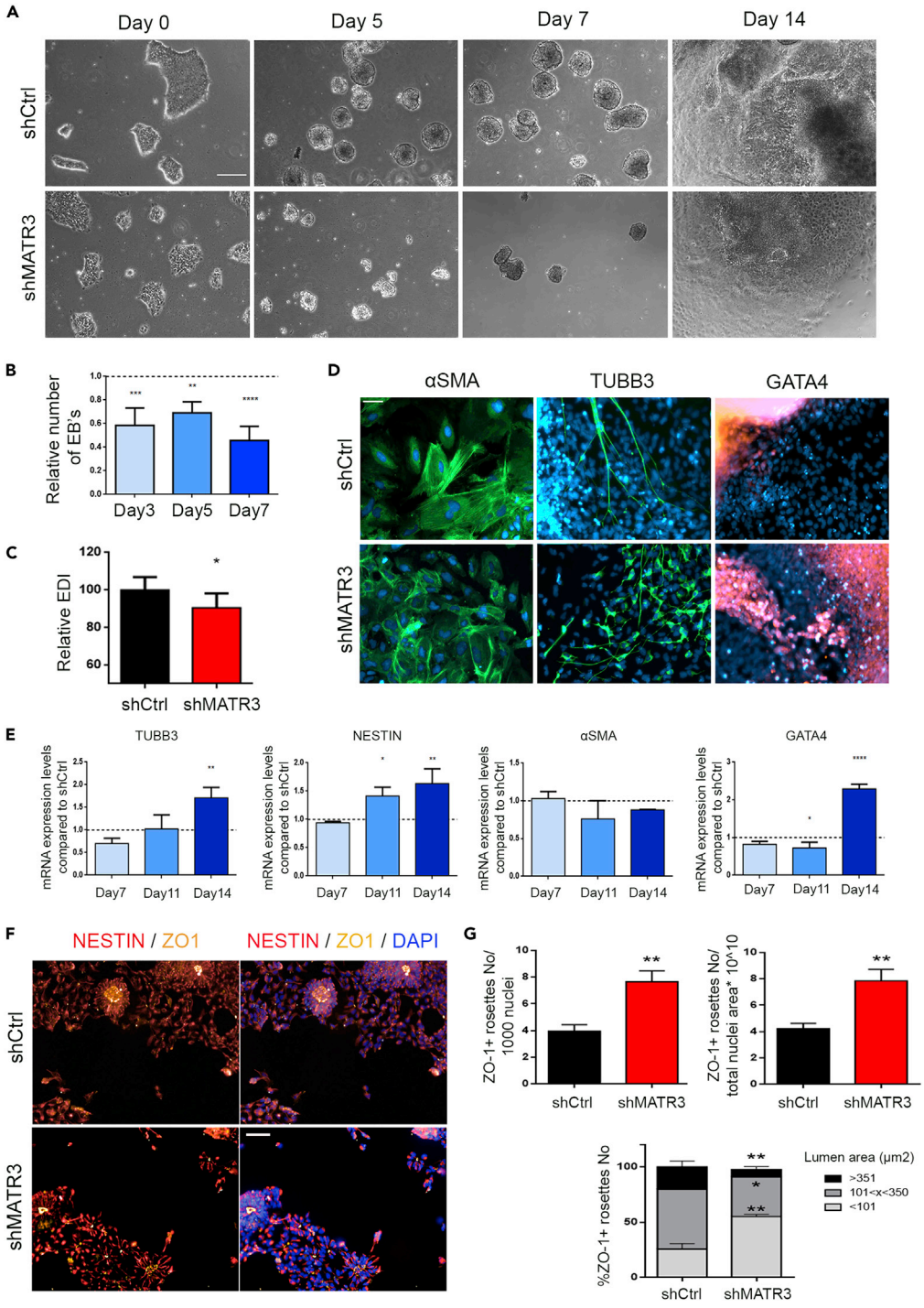

Figure 2. MATR3 is required for hiPSCs' neural differentiation and neuronal maturation

(A) Phase contrast pictures of shCtrl and shMATR3 embryoid body (EB) cultures at specific time points (scale bar, 250 μm).

(B) EBs count analysis performed with Harmony 4.1 software (PerkinElmer) on images acquired with Operetta High Content Screening System (PerkinElmer) using 2× 0.08NA objective. Data are presented as the mean ± SEM. p value was calculated using one-way ANOVA (**$p < 0.01$; ***$p < 0.001$; ****$p < 0.0001$).

(C) Analysis of the elongation distortion index (EDI), a derivative of circularity (EDI = 1/Circularity − 1). Data are presented as the mean ± SEM. p value was calculated using *t* test (*$p < 0.05$).

(D) Immunofluorescence staining for germ layer markers performed on 14 days of EB cultures. EBs were stained for α-SMA (Mesoderm), TUBB3 (Ectoderm), and GATA-4 (Endoderm). Cell nuclei were stained with DAPI (blue). Scale bar, 50 μm.

Figure 2. *Continued*

(E) qRT-PCR analysis performed on 14 days of EB cultures. Values are normalized on the internal housekeeping (β-ACTIN) and reported in comparison with shCtrl samples (reported at value 1 in the graph). Results for NESTIN and TUBB3, α-SMA, and GATA-4 transcripts are presented as mean ± SEM. p value was calculated by one-way ANOVA (*p < 0.05; **p < 0.01; ****p < 0.0001).

(F) Immunofluorescent pictures of Day 12 neuralized shCtrl- and ShMATR3-hiPSC cultures. Neural rosettes' lumens are immunoreactive for ZO-1, and NPCs are stained for Nestin. Scale bar, 50 μm.

(G) (Top) Quantification of ZO-1+ rosettes number (on 1,000 nuclei or on total nuclei area (*10^{10})). (Bottom) The percentage of the number of ZO-1+ rosettes having lumen area (x) >351, 101<x<350 or <100 μm^2. Quantification was done using Columbus software. Statistical analysis was presented as mean ± SEM of three biological replicates. p value was calculated by *t* test (*p < 0.05; **p < 0.01).

role in the polarization process leading to the neural rosette cytoarchitecture and that its absence affects the subsequent terminal neuronal maturation progression.

MATR3 downregulation decreases the expression level of OCT4, NANOG, KLF4, and *LIN28A*

As we observed that MATR3 downregulation impairs single-cell growth and alters lineage commitment during EBs differentiation and neuralization, we reasoned that this might be the consequence of altered pluripotency circuitries. Analysis of the transcript and protein expression levels for several pluripotency determinants revealed that MATR3 downregulation in hiPSCs leads to decreased levels of OCT4, NANOG, and KLF4 (Figures 3A, 3B, S3A, and S3B), but not of SOX2. We also observed a significant decrease in *LIN28A* mRNA levels and only a faint reduction of the protein amount (Figures 3A, 3B, S3A, and S3B). Noteworthy, restoration of MATR3 levels in shMATR3 hiPSCs ultimately rescued the expression of the pluripotency markers (Figures 3C and 3D) and the ability of shMATR3 cells to grow in sub-optimal conditions (Figures S3C and S3D), suggesting a specific role for MATR3 in their regulation. These data indicate that MATR3 contributes to safeguarding the expression levels of several pluripotency regulators, likely by modulating distinctive molecular mechanisms.

MATR3 is associated with the translation machinery and RNA processing

To investigate how MATR3 could fine-tune the pluripotency circuitry, we explored total cell MATR3 interactome by evaluating its binding partners in parental hiPSCs. Immunoprecipitation of MATR3 and subsequent tandem mass spectrometry (IP-MS) led to the identification of MATR3-associated proteins in hiPSCs (Figure 4A). Immunoblot analysis of the immunoprecipitated fractions confirmed MATR3 enrichment. In contrast, no MATR3 was detected in the IgG immunoprecipitated lysates, confirming the specificity of the assay (Figure 4B). We found 151 proteins that were at least 1.5-fold enriched over IgG ($p \leq 0.05$) (Figure 4C, Table S1, Figure S4). Among them, we uncovered several proteins involved in RNA metabolic processes, including alternative splicing, mRNA stability, transcription, and RNA translocation (Table S1, Figures S4A and S4B). The dataset included some known MATR3-interacting RBPs including RALY (Tenzer et al., 2013); PTBP1, which plays a role in alternative splicing (Coelho et al., 2015); DHX9; and HNRNPK, which have been proposed to interact with MATR3 and regulate RNA processing (Salton et al., 2011). We also observed a protein-protein interaction with nucleopore proteins (NUP-205, NUP-93) that can suggest the mechanism by which MATR3 shuttles from the nucleus. In addition, several proteins involved in the translational machinery were found to be enriched, including EIF4A1, EIF4A3, EIF3CL, EIF3D, and EIF3F (Table S1), along with RBPs involved in the process of translation such as L1TD1 (Närvä et al., 2012) and IGF2BP1, one of the readers of m6A modification (Deng et al., 2018). Indeed, a functional enrichment analysis of Gene Ontology categories within this dataset showed significant enrichment in terms related to translation, mRNA surveillance, and ribosome components (Figure 4D and Table S2). Accordingly, protein-protein interaction network analysis revealed that MATR3 interactors group into a distinct Cytoplasmic/Translation cluster, which includes ribosomal subunits and translation initiation factors (Figure 4E and Table S3). Overall, MATR3 protein interactome suggests a pleiotropic role of this protein in hiPSC nuclear RNA metabolism and a previously unrecognized role in the cytoplasm, specifically at the translation apparatus.

MATR3 regulates the translation efficiency of LIN28A, NANOG, and SOX2 mRNAs

IP-MS results support a putative new role for MATR3 in the control of protein synthesis in the cytoplasm. To better investigate this issue, we performed a confocal imaging analysis that revealed a partial localization of MATR3 in the cytoplasm (Figure 5A). Quantitative analysis showed that 25% of total MATR3 immunoreactive spots are in the cytoplasm (Figure S5A). However, this result is overestimating the amount of

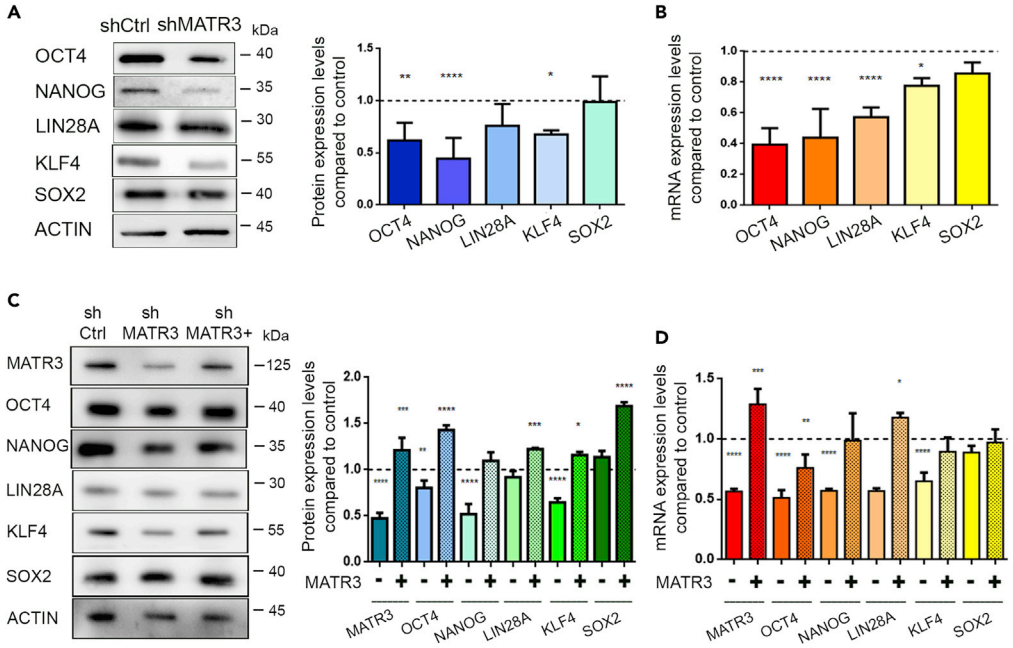

Figure 3. MATR3 downregulation affects the expression levels of pluripotency determinants

(A and B) WB and qRT-PCR analyses for OCT4, NANOG, KLF4, and LIN28A performed on shMATR3-and shCtrl-hiPSC cultures. WB and RT-qPCR results were normalized on the internal housekeeping (β-ACTIN) and reported in comparison to the shCtrl samples (reported as value 1 in the graph). Both analyses were presented as the mean ± SEM of three biological replicates. p value was calculated by one-way ANOVA (*p < 0.05; **p < 0.01; ****p < 0.0001).

(C and D) WB and RT-qPCR analyses for OCT4, NANOG, KLF4, and LIN28A performed on shCtrl-, shMATR3- (–), shMATR3- and on MATR3 rescued shMATR3- (+) cultures. WB and qRT-qPCR analyses were normalized on the internal housekeeping (β-ACTIN) and reported in comparison to the shCtrl values (reported as value 1 in the graph). Values as reported as mean ± SEM. p value was calculated by one-way ANOVA (*p < 0.05; **p < 0.01; ***p < 0.001; ****p < 0.0001).

cytoplasmic MATR3 as the real number of nuclear MATR3 spots is hardly detectable, due to the high presence of MATR3 in the nucleus. The quantification of MATR3 fluorescence intensity in the cytosol and in the nucleus revealed that about 17% of the entire MATR3 fluorescence intensity derived from cytoplasmic MATR3 (Figure S5B). Importantly, this analysis shows that MATR3 maintained a comparable cell distribution in shCtrl and shMATR3 cell lines (Figures S5C and S5D) suggesting that its downregulation did not affect specifically either nuclear or cytoplasmic functions.

To validate IP-MS experiment and evaluate the presence of MATR3 with the translational machinery, we performed confocal images of MATR3 and EIF3A and EIF3C, components of the eIF3 complex that is required for the initiation of protein synthesis (Masutani et al., 2007) (Figures 5B and 5E). Co-localization analysis performed on 3D (x,y,z) revealed that about 20% of cytoplasmic MATR3 signal co-localizes with the eIF3 proteins (Figure S5F). As the high concentration of the EIF3 proteins in the cytoplasm makes the co-localization uncertain, we used, β-ACTIN, another highly abundant cytoplasmic protein, as negative control. In this case, only a few spots were double-positive (Figures S5G and S5H) suggesting that our previous co-localizations were EIF3 specific. Next, by evaluating *de novo* protein synthesis, we investigated the role of MATR3 in translation and whether its downregulation affected global translation. O-propargyl-puromycin (OPP) incorporation assays revealed a marginal reduction of *de novo* protein synthesis in shMATR3 cells (Figure 5C). To explore the potential interaction of MATR3 with the components of the translational machinery, we performed polysome profiling after sucrose gradient fractionation of shCtrl cytoplasmic lysate (Panda et al., 2017). In agreement with our proteomics analysis of MATR3 interactors, we observed that a subpopulation of MATR3 co-sediments with ribosomes and polysomes in control cells (Figure 5D). We ruled out the possibility that MATR3 signal is caused by nuclear contamination of the cytoplasmic lysates, performing a control co-sedimentation analysis of Histone 3 (H3) (Figure S5I). Comparing the polysome profiles in shCtrl and shMATR3 conditions (Figure 5E), we observed an increase of the 80S upon MATR3 silencing. We quantified this effect, calculating the fraction of ribosomes in polysomes in both conditions, finding that when

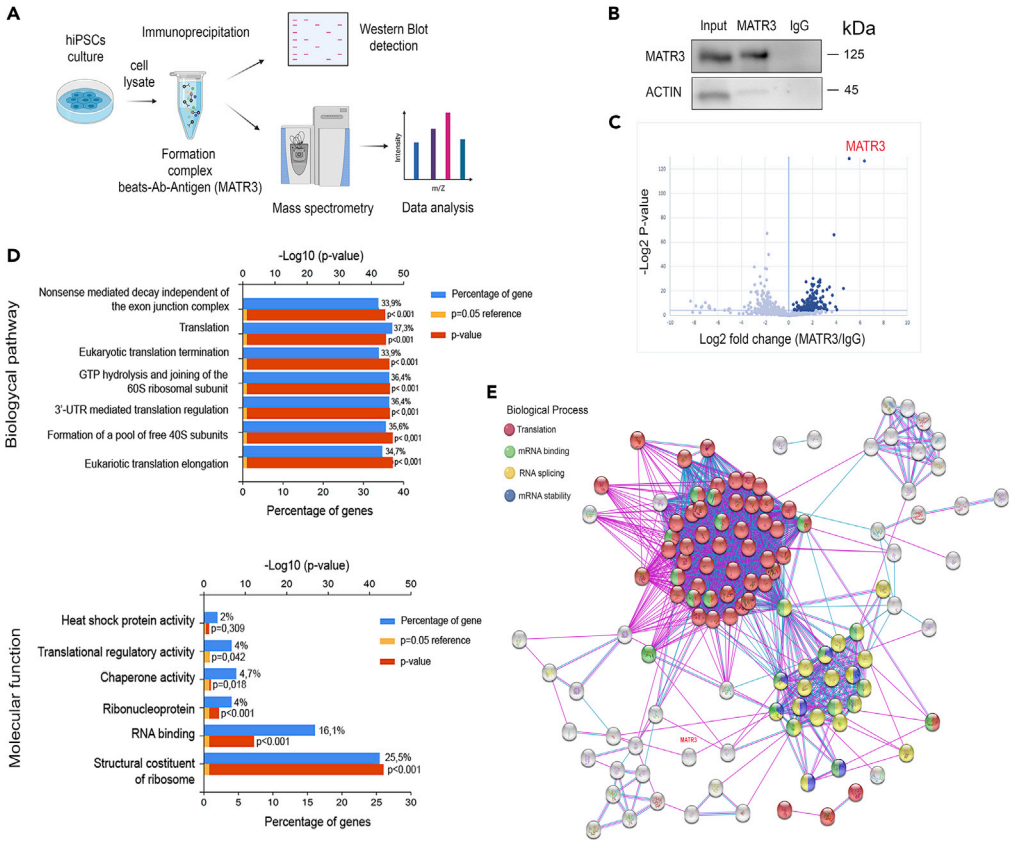

Figure 4. MATR3 is associated to the translational machinery and RNA processing

(A) Schematic representation of the strategy used for the identification of MATR3 interactors. (B) WB performed on parental hiPSC cell lysates co-immunoprecipitated with MATR3 antibody (ab) and IgG as control. Inputs are also shown (Input). The β-ACTIN signal is present only in the input sample confirming the specificity of MATR3 antibody.

(C) Volcano plot representation of MS analysis results. The ScatterPlot showed 151 proteins significantly enriched in MATR3 (dark blue dots, right of the graph) versus IgG pulldown (left part of the graph), with a *t* test p value < 0.05 (or > 4.32 when −log2 transformed).

(D) Functional enrichment analysis of MATR3 interactors conducted by FunRich software. Two different GO biological processes analyses, Biological pathway and Molecular function, were used. Significance of the interactions is represented by a red histogram, $p < 0.001$ (orange with minimum $p < 0.05$), and the percentage of overrepresentation of the genes is represented by a blue bar.

(E) Protein-protein interactions calculated by STRING interaction database. Only high confidence interactions (interaction score >0.7), as determined by the STRING database, were accepted. Each node represents a protein, and edges represent protein-protein associations. In the graph, proteins involved in translation (red plot), mRNA processing (green plot), RNA splicing (yellow plot), and mRNA stabilization (blue plot) are reported.

MATR3 is downregulated, this value increased. Although this change is limited and not statistically significant, the trend suggests that reduced MATR3 expression has a translational effect, as also observed in the reduction of *de novo* protein synthesis observed in OPP assays of shMATR3 iPS cells (Figure 5C). To further investigate if MATR3 may play a translational role in regulating specific genes as the pluripotency factors at the translation level, we performed a co-sedimentation analysis of *OCT4, KLF4, LIN28A, NANOG,* and *SOX2* mRNAs in shCtrl and shMATR3 iPS cells. Our results showed that, in shMATR3 cells, *OCT4, LIN28A,* and *NANOG* mRNAs shift from heavier to lighter fractions along the profile, suggesting a possible defect in the recruitment of these mRNAs on polysomes (Figure 5F). Taken together, these data suggest that a portion of cytoplasmic MATR3 protein is associated with the translational apparatus and that its absence affects global translation only marginally. However, MATR3 downregulation induced a decrease in the loading on polysomes of mRNAs encoding for *OCT4, LIN28A,* and *NANOG* pluripotency factors. Taken together, these data suggest that the presence of MATR3 on the translation apparatus is necessary to favor the polysomal loading of a specific subset of mRNAs.

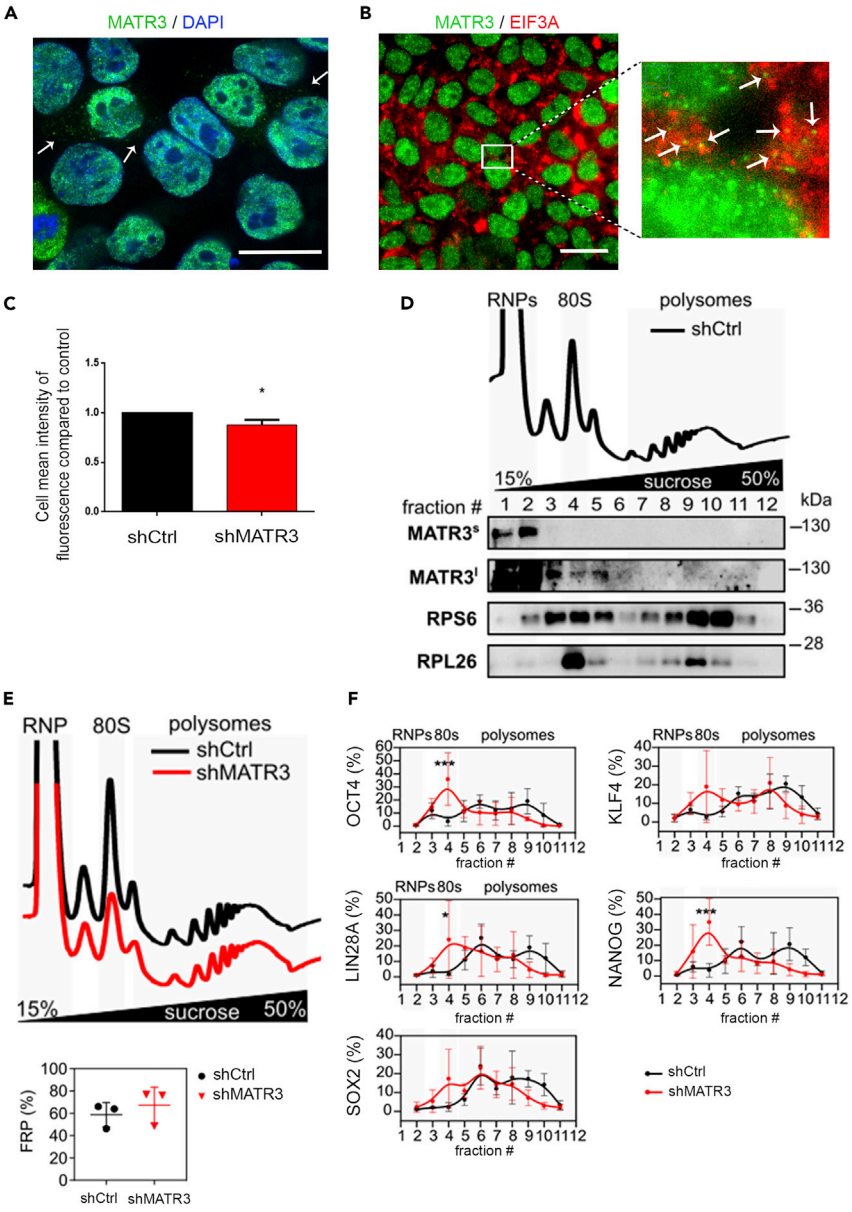

Figure 5. MATR3 regulates the translation efficiency of OCT4, LIN28A, and NANOG mRNAs

(A) Immunofluorescence pictures to detect the subcellular localization of MATR3 in hiPSCs. Scale bar, 20 μm.

(B) Pictures of hiPSCs stained for MATR3 (green signal) and eIF3a (red signal). Nuclei were stained with DAPI (blue signal). Scale bar, 20 μm. Zoom highlights an overlight between MATR3-EIF3A (orange spots).

(C) Evaluation of *de novo* protein synthesis measured by O-propargyl-puromycin (OPP) Alexa Fluor 488 incorporations. Quantification performed by Operetta High Content Screening System. Data presented as mean ± SEM of three biological replicates. shMATR3 values are compared with shCtrl (reported as value 1). The statistical significance was calculated by *t* test, 95% of confidence.

(D) Polysome profiling performed on shCtrl hiPSC and co-sedimentation profiles of MATR3 and ribosome markers RPS6 and RPL26. The signal of MATR3 along the profile is shown for short ($MATR3^s$) and long ($MATR3^l$) exposure times of acquisition. A single biological replicate is shown.

(E) Polysomal profiles of shCtrl and shMATR3 hiPSC and comparison between FRP in shCtrl and shMATR3 (shCtrl: n = 3, shMATR3: n = 3). No significant changes identified with paired two-tailed t test ($p = 0.1075$).

(F) qRT-PCR analysis for *SOX2, OCT4, LIN28A, NANOG*, and *KLF4* performed on mRNA from fractions obtained from the polysome profiling. Statistical analysis was performed on the mean of three biological replicates, two-way ANOVA (*$p < 0.05$; ***$p < 0.001$).

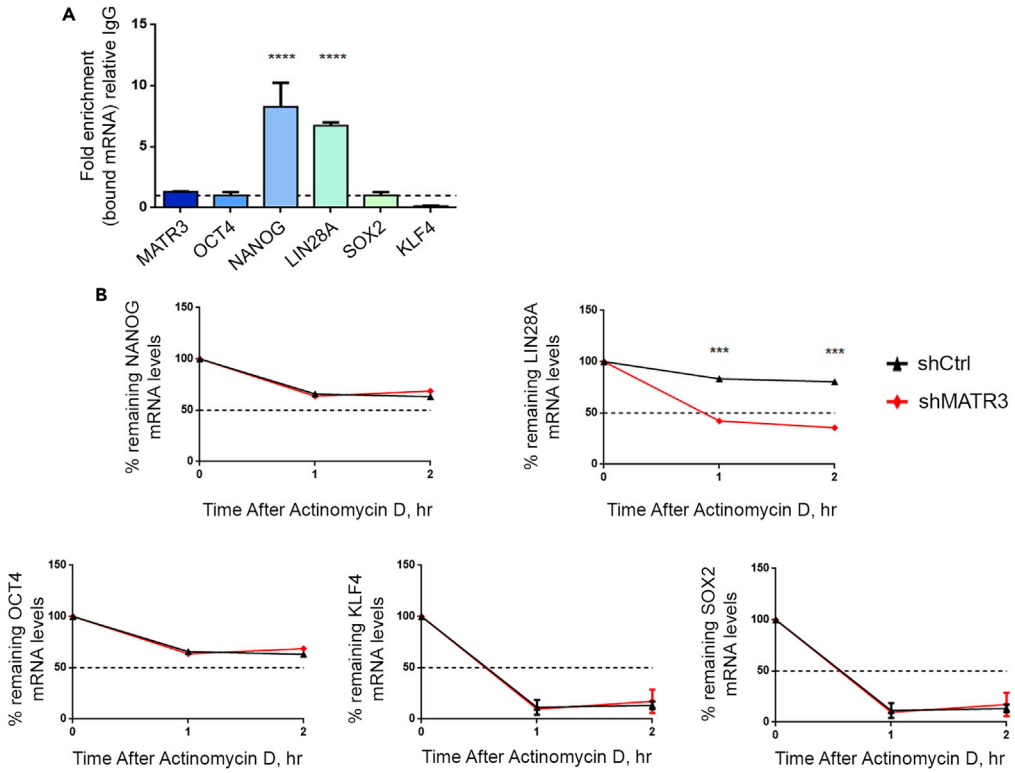

Figure 6. MATR3 stabilizes *NANOG* and *LIN28A* mRNAs

(A) MATR3 RNA immunoprecipitation (RIP) performed on parental hiPSCs followed by qRT-PCR analysis. Fold enrichment was relative to IgG. Values are presented graphically as mean ± SEM from three biological replicates. One-way ANOVA (****$p < 0.0001$).

(B) qRT-PCR analysis for the evaluation of mRNA half-lives in shCtrl and shMATR3 hiPSCs performed by actinomycin-D assay. qRT-PCR values are normalized to their internal housekeeping (β-ACTIN). Results are expressed as percentages of mRNA abundance relative to Time 0. Statistical analysis was performed on the mean of three biological replicates, two-way ANOVA (***$p < 0.001$).

MATR3 stabilizes *NANOG* and *LIN28A* mRNAs

To understand whether translation efficiency was linked to MATR3 RNA-binding ability, we investigated which of the pluripotency regulators transcripts among *OCT4, NANOG, LIN28A, SOX2,* and *KLF4* were directly bound by MATR3. RNA immunoprecipitation (RIP) of endogenous MATR3 in parental hiPSCs and analysis of the abundance of transcripts by qPCR revealed that MATR3 significantly binds to *NANOG* and *LIN28A* mRNAs (Figure 6A). Interestingly, the same result was not seen for *OCT4, SOX2,* and *KLF4,* suggesting that changes in their transcript levels, observed during MATR3 downregulation, are likely dependent on indirect molecular mechanisms. MATR3 binds hundreds of transcripts contributing to the stabilization of some of them, including *HTLF* (*FOXN2*) and *HNT* (*RREB1*) (Salton et al., 2011). We measured the mRNA half-lives of pluripotency regulators by arresting their *de novo* RNA synthesis in shCtrl- and shMATR3-hiPSCs (Figure 6B). MATR3 silencing led to significant reductions in *NANOG* ($p<0.05$ at 1 h time point) and *LIN28A* ($p<0.05$ at 1 h) mRNA half-lives, but did not affect *OCT4, SOX2,* and *KLF4* transcripts half-lives (Figures 6B and S6). These results indicate that MATR3 regulates the mRNA levels of *NANOG* and *LIN28A* by increasing their stability via direct binding, thus protecting these transcripts from degradation. Coherently, half-lives of the *OCT4, SOX2,* and *KLF4* transcripts, which are not bound by MATR3, are not affected by MATR3 downregulation.

MATR3 sustains OCT4 expression by regulating *YTHDF1* expression

We then sought to understand whether MATR3 could regulate these factors at the transcriptional level (Skowronska-Krawczyk et al., 2014). In rat pituitary cells (GC cells), ChIP sequencing (ChIP-seq) using a matrin-3 antibody, revealed that matrin-3 binds to DNA regulatory sequences, by physically interacting with

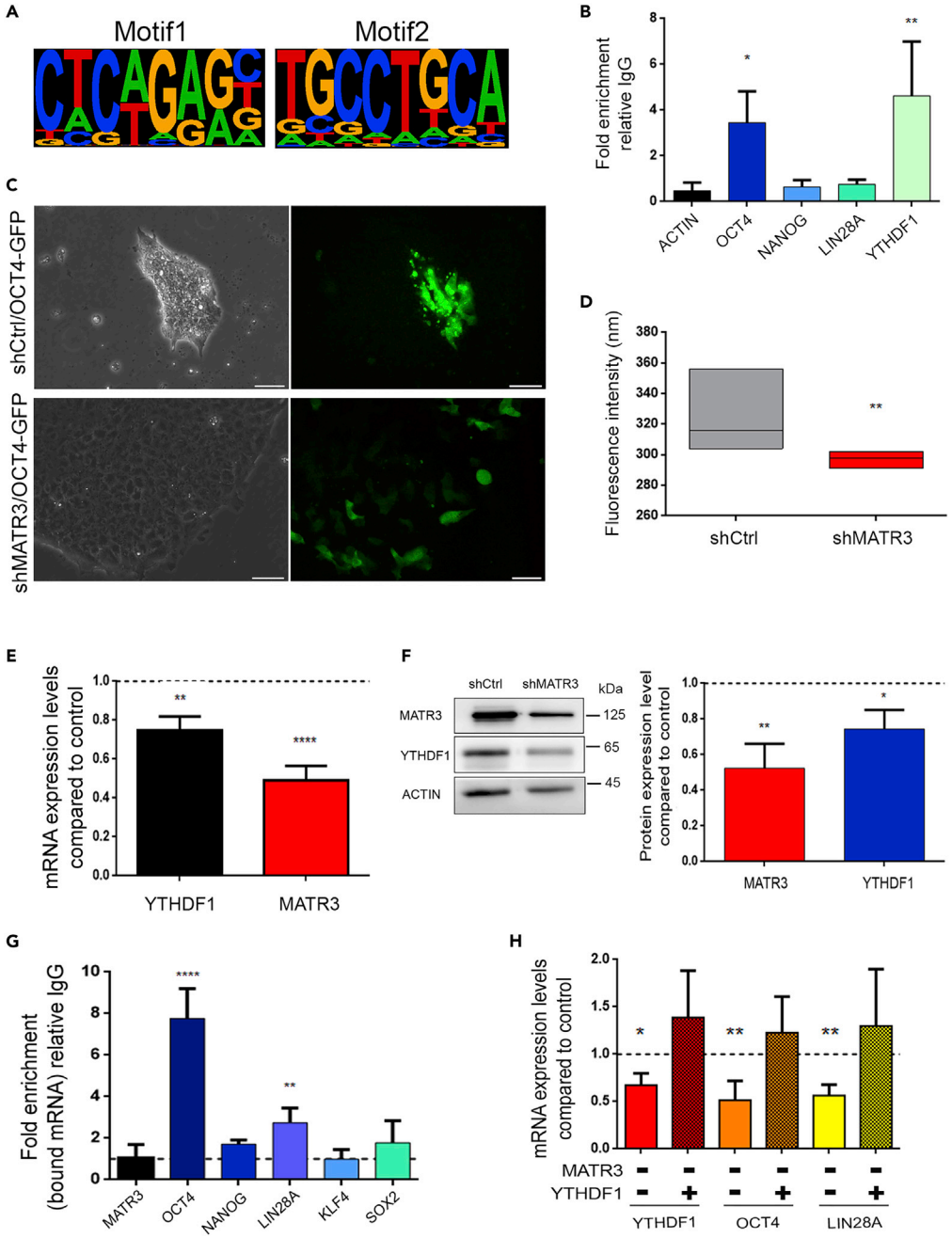

Figure 7. MATR3 regulates OCT4 expression by binding to its promoter and by regulating YTHDF1 transcription

(A) Highest scoring motifs analysis (best motif on the left, and second-best on the right) on the 500 DNA sequences most significantly bound by MATR3 according to ChIP-seq assay (Skowronska-Krawczyk et al., 2014), obtained with HOMER (Heinz et al., 2011).

(B) Chromatin immunoprecipitation (ChIP) on ACTIN, OCT4, NANOG, LIN28A, and YTHDF1 promoters performed using antibodies against MATR3 and IgG as the negative control. Data were normalized to non-immunoprecipitated samples (INPUT) and compared with the IgG sample. OCT4 and YTHDF1 promoters showed a region predicted to contain the MATR3 DNA consensus sequence; reported as mean ± SEM. p value values were calculated by one-way ANOVA (*$p < 0.05$; **$p < 0.01$).

(C) Generation of stable hiPSC line expressing green fluorescent protein (GFP) under control of the OCT4 promoter. hiPSCs OCT4-GFP stably infected with shMATR3 and shCtrl lentiviral vectors. Scale bar, 50 μm.

Figure 7. *Continued*

(D) shMATR3/OCT4-GFP fluorescence intensity was quantified and compared with shCtrl/OCT4-GFP. The quantification of immunofluorescence intensity was performed using the ImageJ mean fluorescence intensity measurement. Data are reported as mean ± SEM for three biological replicates; p value was calculated using a t test (**p < 0.01).

(E) qRT-PCR analyses of YTHDF1 in shMATR3 hiPSCs compared with shCtrl cells. Values are normalized on internal housekeeping (β-ACTIN) and reported in comparison to shCtrl values (reported as value 1 in the graph). The mean ± SEM of three biological replicates are reported. p value was calculated by one-way ANOVA (**p < 0.01; ****p< 0.0001).

(F) Left: Representative WB of MATR3 and YTHDF1 in shMATR3 hiPSCs compared with shCtrl cells. Right: densitometric analysis of three biological replicates. Values are normalized on internal housekeeping (β-ACTIN) and reported in comparison to shCtrl values (reported as value 1 in the graph). The mean of three biological replicates are reported. p value was calculated by one-way ANOVA (*p < 0.05; **p < 0.01).

(G) RIP using the YTHDF1 antibody in the Gibco cell line (A18945), followed by RT-qPCR. Fold enrichment was relative IgG. Represented graphically as mean ± SEM of three biological replicates. One-way ANOVA (***p < 0.001; ****p < 0.0001).

(H) RT-qPCR analyses of YTHDF1, OCT4, and LIN28A, on shMATR3(−) cells rescued with overexpression of YTHDF1 (YTHDF1 +) cultures. RT-qPCR analyses were normalized on internal housekeeping (β-ACTIN) and reported in comparison to shCtrl values (reported as value 1 in the graph). Values are reported as mean ± SEM. p value was calculated by One-way ANOVA (*p < 0.05, **p < 0.01).

the Pou1f1 transcription factor and contributes to its activity (Skowronska-Krawczyk et al., 2014). Inspection of Chip-seq peaks revealed that their genomic positions corresponded mainly to distal regions from the transcription start sites (Table S4). Notably, a fraction was directly associated with promoter regions, including the binding sequence of the Pou family, as described in the original (Skowronska-krawczyk et al., 2015). Functional analysis performed on members of this list revealed that MATR3 was mainly present in promoter regions of genes involved in the development, stemness, and stem cell proliferation processes (Figures S7A and S7B and Table S4). Indeed, we found notable examples of genes regulating embryo development including *Shh* (sonic hedgehog signaling molecule) (Blaess et al., 2015; Haraguchi et al., 2001; Tickle et al., 2017; Weed et al., 1997), Sox factors (*Sox4, Sox5, Sox11*) (Bowles et al., 2000; Potzner et al., 2010; Sarkar and Hochedlinger, 2014; She and Yang, 2015), and Wnt signalling (*Sfrp2, Wnt7a*) (Hao et al., 2006; Kele et al., 2012; Miao et al., 2018; Ren et al., 2018). We then shortlisted the first most significant 500 ChIP-seq peak sequences, ordered according to peak score, and obtained the two best MATR3 DNA-binding motifs by using HOMER (Figure 7A). Comparing these motifs to available databases we could not find any obvious matching (Table S4). We examined the *LIN28A*, *NANOG*, *SOX2*, *KLF4*, and *OCT4* transcriptional start site (TSS) upstream regions and checked for the presence of the MATR3 DNA-binding consensus sequence. We did not find any consensus sequence on these genes, but on *OCT4* (Table S5, 114 significant putative binding sequences). Experimental validation by ChIP assay in hiPSCs using the anti-MATR3 antibody confirms the enrichment of MATR3 on the *OCT4* promoter, but we did not report any enrichment of MATR3 in the *NANOG* and *LIN28A* upstream TSS regions (Figure 7B). To confirm MATR3 role in *OCT4* transcription, we used a stable hiPSC line expressing GFP under the control of *OCT4* promoter (hiPSCs OCT4-GFP). Indeed, stable MATR3 silencing (shMATR3/OCT4-GFP cell line) (Figure 7C) showed strong loss of GFP fluorescence when compared with shCtrl/OCT4-GFP, highlighting the importance of MATR3 in regulating *OCT4* transcription (Figures 7C and 7D).

Transcript levels of the stemness regulators, including *OCT4, LIN28A, SOX2,* and *NANOG* mRNAs, can also regulated by m6A methylation (Chen et al., 2015b). Thus, by RIP using anti-m6A antibody (MeRIP), *OCT4* and *LIN28A* transcripts show a more than 20- and 6-fold enrichment in methylation over the IgG background, respectively (Figure S7C). We searched for the MATR3-DNA-binding consensus in promoter regions of genes involved in the m6A machinery and found enrichment in the promoters of all the genes involved in m6A regulation (Table S5). We focused our attention on *YTHDF1* that was the gene with the highest presence of predicted MATR3-binding elements in its promoter (123 significant binding sequences). Indeed, experimental validation of computational predictions by ChIP indicated that MATR3 bound to the *YTHDF1* promoter region (Figure 7B). In accordance with a transcriptional-mediated regulation of *YTHDF1*, we found both YTHDF1 mRNA and protein expression levels decreased in shMATR3 hiPSCs (Figures 7E and 7F). In addition, YTHDF1 bound to *OCT4* and *LIN28A* methylated transcripts but not to *SOX2, KLF4,* and *NANOG*, by RIP (Figure 7G), suggesting that these two transcripts are under the direct regulation of YTHDF1. Indeed, this RNA-binding protein binds to m6A-methylated RNAs and regulates their metabolism, generally promoting their translation (Wang et al., 2015). Noteworthy, restoration of YTHDF1 levels in shMATR3 hiPSCs rescued both *OCT4* and *LIN28A* transcript levels (Figure 7H), suggesting

the presence of a regulatory loop by which MATR3 triggers the expression of YTHDF1 that, in turn, regulates the metabolism of the *OCT4* and *LIN28A* transcripts.

DISCUSSION

In this work, we spotted a crucial role of MATR3 in maintaining the pluripotency circuitry by reporting novel and pleiotropic functions. We found that MATR3 fine-tunes pluripotency regulators' expression at the post-transcriptional level by regulating their translational efficiency (NANOG, LIN28A, and SOX2) and mRNA stabilization (NANOG and LIN28A). In addition, we found that MATR3 binds to *OCT4* and *YTHDF1* promoter regions regulating their mRNAs transcription, and, finally, YTHDF1 maintains the expression level of m6A OCT4 and LIN28A mRNAs. The relevance of MATR3 in pluripotency was observed in stressful conditions, as its absence impaired single cell growth and colony formation. Indeed, we observed altered phenotypes in shMATR3 hiPSCs during pluripotency exit and lineage commitment as assessed by the EB formation assay, showing both abnormal EB size and number and impaired expression of trilineage markers. These effects could be ascribed to the reduced capability of shMATR3 cells to survive and efficiently aggregate following dissociation to form regular EBs. Accordingly, shMATR3 EBs exhibited an irregular structure that could be responsible for altered axis formation in EBs, resulting in an impaired germ layer specification (Fuchs and Pasteiner, 2012). Altered phenotypes were also observed in specific neural induction conditions, where MATR3-silenced cultures showed an increase in the number of neural rosettes and decreased lumen's size. Proper neural rosette's cytoarchitecture and size have been shown to be the direct consequence of a precise balance between self-renewal and differentiation and are mandatory for the correct neuronal differentiation/maturation (Curchoe et al., 2012; Temple, 2001). Coherently, morphometric analyses showed a reduced number of neurites and neurite arborization, in shMATR3 hiPSC-derived neurons. These results are consistent with a recent report describing that MATR3 knockdown results in disordered *in vitro* differentiation of mouse NSCs into neurons, causing the collapse of the developing mouse cerebral cortical layer structure *in vivo* (Niimori-kita et al., 2018).

Although MATR3 is predominantly a nuclear protein, our proteomic investigation suggested a role of MATR3 in the cytoplasm. The binding to nucleopore proteins may indicate the mechanism by which MATR3 conveys its RNA cargo from the nucleus to the cytoplasm, supporting defects of mRNA transport, possibly, to the translation machinery, observed with ALS-related mutated MATR3 in NSC-34 cells (Boehringer et al., 2017). Indeed, the binding to the eukaryotic initiation factors of the multiprotein eIF3, required for the binding of mRNAs to the 40S ribosomal subunit to form the 43S preinitiation complex (Hershey et al., 2012; (Marchione et al., 2013)), underlined a possible role in the translation. In addition, besides detecting previously reported interactors including DHX9, which forms a complex with HNRNPK acting in RNA splicing and translation (Salton et al., 2011), we also found novel interactors specifically involved in the translation of genes regulating stemness competence. Among them, we found L1TD1, an RBP that is expressed in iPSCs, whose promoter is bound by OCT4, NANOG, and SOX2 and that regulates pluripotency maintenance via direct binding to LIN28A (Emani et al., 2015; Närvä et al., 2012). Indeed, polysome profiling results indicate MATR3 main association with the monosome fraction, and that MATR3 silencing produces a decrease in the monosome peak. These data may suggest a possible role of MATR3 in the assembly of the 80S complex, which requires further investigation. The mild reduction of *de novo* protein synthesis and the decrease of translational efficiency of specific genes, following MATR3 silencing, suggest that MATR3 is not involved in global transcriptome translation, but rather it specifically regulates the translation of a relevant subset of transcripts. Coherently, mRNAs directly bound by MATR3, such as *NANOG* and *LIN28A*, showed a decrease in transcript stability that can be explained by a MATR3-dependent reduction in ribosome recruitment and polysomal loading. However, we found that transcripts not directly bound by MATR3 also underwent a decrease in polysomal loading, thus suggesting additional indirect effects on translation by MATR3. For example, *SOX2* expression level was not dependent on MATR3, and its transcript was not bound by MATR3. Nevertheless, *SOX2* mRNA exhibited a translation efficiency impairment. On the other side, *KLF4* whose expression level is affected by MATR3 silencing, but was not bound by MATR3, did not show change in its translation efficiency. A different scenario emerged for OCT4, a core pluripotency factor (Shi and Jin, 2010). OCT4 expression was dependent on MATR3 in various manners. MATR3 was found on the *OCT4* promoter suggesting a direct control of the *OCT4* transcript in hiPSCs. Moreover, an indirect regulation by MATR3 was also observed. To this end, we identified a new gene regulatory network, in which MATR3 is essential to sustain *YTHDF1* expression, likely via a transcription-mediated mechanism and, the encoded protein binds to m6A-methylated *OCT4* and *LIN28A* transcripts. YTHDF1 has been shown to play a crucial role in mediating m6A-RNA translation by interacting with

eIF3 and facilitating translation initiation (Wang et al., 2015; Zhuang et al., 2019). Noteworthy, an important role for YTHDF1 in the maintenance of PSCs' pluripotency by binding to m6A JAK2 mRNA has also been reported (Wu et al., 2019). Accordingly, we found that the restoration of YTHDF1 expression in shMATR3-hiPSCs completely rescued the expression level of *OCT4* and *LIN28A*. In summary, our findings reveal the multifaceted role of MATR3 in maintaining the pluripotency circuitry and introduce translation as a new layer of regulation, functionally ruled by this pleiotropic protein.

Limitations of the study

This study has been performed in hiPSCs, therefore a validation in human ESCs is required to generalize the proposed model.

Resource availability

Lead contact

Further information and requests for resources and reagents should be directed to and will be fulfilled by the lead contact, Alessandro Provenzani (alessandro.provenzani@unitn.it).

Materials availability

All unique/stable reagents generated in this study are available from the lead contact with a completed Materials Transfer Agreement.

Data and code availability

The published article includes all datasets generated or analyzed during this study. Supplementary Tables are available at https://data.mendeley.com/drafts/xwx6p86dzj?folder=fed972f6-5de9-4bd4-9155-8804a3279708.

METHODS

All methods can be found in the accompanying transparent methods supplemental file.

SUPPLEMENTAL INFORMATION

Supplemental information can be found online at https://doi.org/10.1016/j.isci.2021.102197.

ACKNOWLEDGMENTS

This work was supported by grants from Fondazione Cassa Di Risparmio Di Trento E Rovereto (Drug repositioning project #40102838) to A. Provenzani and A.Q.; Fondazione ARISLA (project TARGET RAN # 40103385 to A. Provenzani and A. Poletti and project MLOpathy to A. Poletti); Fondazione Cariplo, Italy (n. 2014-0686, # 40102636) to A. Poletti; Fondazione Telethon, Italy (GGP19128 to A. Poletti); Italian Association for Cancer Research (AIRC) grants IG 12869, IG 18985, and IG 21548; Kennedy's Disease Association (2018 grant to R.C.); Italian Ministry of University and Research (MIUR); PRIN - Progetti di ricerca di interesse nazionale (n. 2017F2A2C5 to A. Poletti); Agenzia Italiana del Farmaco (AIFA) (Co_ALS to A. Poletti); and Fondazione Regionale per la Ricerca Biomedica (FRRB) (Regione Lombardia, TRANS_ALS, project nr. 2015-0023, to A. Poletti). The authors wish to thank the Facilities of High Throughput Screening (HTS) and Advanced Imaging for their support in performing the experiments.

AUTHOR CONTRIBUTIONS

Conceptualization, A. Provenzani, L.C., D. Pollini, A. Poletti, G.V., and A.Q.; methodology, D. Pollini, R.L., M.C., G.V., and A. Provenzani; investigation, D. Peroni, R.L., F.M., A.R., M.M., I.B., W.T., N.V.L., V.C., and E.D.; software, E.D.; data curation, D. Pollini and E.D; writing – original draft, D. Peroni and A. Provenzani; writing – review & editing, all authors; visualization, D. Pollini; funding acquisition, A. Provenzani, A.Q., and A. Poletti; resources, L.C., G.V., and M.C.; supervision and project administration, A. Provenzani.

DECLARATION OF INTERESTS

The authors declare no competing interest.

Received: May 18, 2020
Revised: November 22, 2020
Accepted: February 11, 2021
Published: March 19, 2021

REFERENCES

Banerjee, A., Vest, K.E., Pavlath, G.K., and Corbett, A.H. (2017). Nuclear poly (A) binding protein 1 (PABPN1) and Matrin3 interact in muscle cells and regulate RNA processing. Nucleic Acids Res. *45*, 10706–10725.

Batista, P.J., Molinie, B., Wang, J., Qu, K., Zhang, J., Li, L., Bouley, D.M., Lujan, E., Haddad, B., Daneshvar, K., et al. (2014). M6A RNA modification controls cell fate transition in mammalian embryonic stem cells. Cell Stem Cell *15*, 707–719.

Belgraders, P., Dey, R., and Berezneyg, R. (1991). Molecular cloning of matrin 3. J. Biol. Chem. *266*, 9893–9899.

Blaess, S., Szabó, N., Haddad-tóvolli, R., Zhou, X., and Álvarez-bolado, G. (2015). Sonic hedgehog signaling in the development of the mouse hypothalamus. Front. Neuroanat. *8*, 1–6.

Boehringer, A., Garcia-Mansfield, K., Singh, G., Bakkar, N., Pirrotte, P., and Bowser, R. (2017). ALS associated Mutations in matrin 3 alter protein-protein interactions and Impede mRNA nuclear export. Sci. Rep. *7*, 1–14.

Bowles, J., Schepers, G., and Koopman, P. (2000). Phylogeny of the SOX family of developmental transcription factors based on sequence and structural indicators. Dev. Biol. *227*, 239–255.

Chen, T., Hao, Y., Zhang, Y., Li, M., Wang, M., Han, W., and Wu, Y. (2015a). m 6 A RNA methylation is regulated by MicroRNAs and promotes reprogramming to pluripotency article m 6 A RNA methylation is regulated by MicroRNAs and promotes reprogramming to pluripotency. Stem Cell *16*, 289–301.

Chen, T., Hao, Y.J., Zhang, Y., Li, M.M., Wang, M., Han, W., Wu, Y., Lv, Y., Hao, J., Wang, L., et al. (2015b). M6A RNA methylation is regulated by microRNAs and promotes reprogramming to pluripotency. Cell Stem Cell *16*, 289–301.

Coelho, M.B., Attig, J., Bellora, N., Konig, J., Hallegger, M., Kayikci, M., Eyras, E., Ule, J., and Smith, C.W. (2015). Nuclear matrix protein Matrin3 regulates alternative splicing and forms overlapping regulatory networks with PTB. EMBO J. *34*, 653–668.

Curchoe, C.L., Russo, J., and Terskikh, A.V. (2012). HESC derived neuro-epithelial rosettes recapitulate early mammalian neurulation events; an in vitro model. Stem Cell Res *8*, 239–246.

Deng, X., Su, R., Weng, H., Huang, H., Li, Z., and Chen, J. (2018). RNA N 6 -methyladenosine modification in cancers: Current status and perspectives. Cell Res. https://doi.org/10.1038/s41422-018-0034-6.

Emani, M.R., Närvä, E., Stubb, A., Chakroborty, D., Viitala, M., Rokka, A., Rahkonen, N., Moulder, R., Denessiouk, K., Trokovic, R., et al. (2015). The L1TD1 protein interactome reveals the importance of post-transcriptional regulation in human pluripotency. Stem Cell Reports *4*, 519–528.

Fuchs, C., and Pasteiner, W. (2012). Self-organization phenomena in embryonic stem cell-derived embryoid Bodies: Axis formation and breaking of symmetry during Cardiomyogenesis. Cell Tissues Organs, 377–391.

Geula, S., Moshitch-Moshkovitz, S., Dominissini, D., Mansour, A.A., Kol, N., Salmon-Divon, M., Hershkovitz, V., Peer, E., Mor, N., Manor, Y.S., et al. (2015). m6A mRNA methylation facilitates resolution of naïve pluripotency toward differentiation. Science *347*, 0–5.

Guallar, D., and Wang, J. (2014). RNA-binding proteins in pluripotency, differentiation, and reprogramming. Front. Biol. (Beijing). https://doi.org/10.1007/s11515-014-1326-y.

Hao, J., Li, T., Qi, X., Zhao, D., and Zhao, G. (2006). WNT/h -catenin pathway up-regulates Stat3 and converges on LIF to prevent differentiation of mouse embryonic stem cells. Dev. Biol. *290*, 81–91.

Haraguchi, R., Mo, R., Hui, C., Motoyama, J., Makino, S., Shiroishi, T., Gaffield, W., and Yamada, G. (2001). Unique functions of Sonic hedgehog signaling during external genitalia development. Development *128*, 4241–4250.

Hershey, J.W.B., Sonenberg, N., and Mathews, M.B. (2012). Principles of translational control: an overview. Cold Spring Harb. Perspect. Biol. *4*, a011528.

Hisada-Ishii, S., Ebihara, M., Kobayashi, N., and Kitagawa, Y. (2007). Bipartite nuclear localization signal of matrin 3 is essential for vertebrate cells. Biochem. Biophys. Res. Commun. *354*, 72–76.

Huang, H., Weng, H., Sun, W., Qin, X., Shi, H., Wu, H., Zhao, B.S., Mesquita, A., Liu, C., Yuan, C.L., et al. (2018). Recognition of RNA N 6 -methyladenosine by IGF2BP proteins enhances mRNA stability and translation. Nat. Cell Biol. *20*, 285–295.

Jha, B.S., Rao, M., and Malik, N. (2015). Motor neuron differentiation from pluripotent stem cells and other Intermediate proliferative Precursors that can be discriminated by lineage specific reporters. Stem Cell Rev. Rep. *11*, 194–204.

Johnson, J.O., Pioro, E.P., Boehringer, A., Chia, R., Feit, H., Renton, A.E., Pliner, H.A., Abramzon, Y., Marangi, G., Winborn, B.J., et al. (2014). Mutations in the Matrin 3 gene cause familial amyotrophic lateral sclerosis. Nat. Neurosci. *17*, 664–666.

Kele, J., Andersson, E.R., Villaescusa, J.C., Cajanek, L., Parish, C.L., Bonilla, S., Toledo, E.M., Bryja, V., Rubin, J.S., Shimono, A., and Arenas, E. (2012). SFRP1 and SFRP2 dose-dependently regulate midbrain dopamine neuron development in vivo and in embryonic stem cells. Stem Cells *30*, 865–875.

Leblond, C.S., Gan-Or, Z., Spiegelman, D., Laurent, S.B., Szuto, A., Hodgkinson, A., Dionne-Laporte, A., Provencher, P., de Carvalho, M., Orrù, S., et al. (2016). Replication study of MATR3 in familial and sporadic amyotrophic lateral sclerosis. Neurobiol. Aging *37*, 209.e17–209.e21.

Leong, C., Zhai, D., Kim, B., Yun, S., and Chang, Y. (2013). ScienceDirect Neural stem cell isolation from the whole mouse brain using the novel FABP7-binding fluorescent dye, Cdr3. Stem Cell Res. *11*, 1314–1322.

Lin, Y., Chen, G., Engineering, G., and Facility, C. (2014). Embryoid Body Formation from Human Pluripotent Stem Cells in Chemically Defined E8 Media (Harvard Stem Cell Institute), pp. 1–4.

Lin, K., Tsai, P., Liao, Y., Chen, W., Tsai, C., Soong, B., and Lee, Y. (2015). Neurobiology of Aging Mutational analysis of MATR3 in Taiwanese patients with amyotrophic lateral sclerosis. Neurobiol. Aging *36*, 2005.e1–2005.e4.

Marangi, G., Lattante, S., Doronzio, P.N., Conte, A., Tasca, G., Monforte, M., Patanella, A.K., Bisogni, G., Meleo, E., La Spada, S., et al. (2017). Matrin 3 variants are frequent in Italian ALS patients. Neurobiol. Aging *49*, 218.

Marchione, R., Leibovitch, S.A., and Lenormand, J. (2013). The translational factor eIF3f: the ambivalent eIF3 subunit. Cell Mol. Life Sci. *70*, 3603–3616, https://doi.org/10.1007/s00018-013-1263-y.

Masutani, M., Sonenberg, N., and Yokoyama, S. (2007). Reconstitution reveals the functional core of mammalian eIF3. EMBO J. *26*, 3373–3383.

Miao, N., Bian, S., Lee, T., Mubarak, T., Huang, S., and Wen, Z. (2018). Opposite roles of Wnt7a and Sfrp1 in modulating proper development of neural progenitors in the mouse cerebral Cortex. Front. Mol. Neurosci. *11*, 1–14.

Närvää, E., Rahkonena, Nelly, Maheswara Reddy Emania, R.L., Huha-Pekka, P., Nästia, J., Autioa, R., Rasoola, O., Denessiouka, K., Harri, L., Raod, A., and Lahesmaaa, R. (2012). RNA-binding protein L1TD1 interacts with LIN28 via RNA and is required for human embryonic stem cell self-renewal and Cancer cell proliferation. Stem Cells *30*, 452–460.

Niimori-kita, K., Tamamaki, N., Koizumi, D., and Niimori, D. (2018). Matrin-3 is essential for fibroblast growth factor 2-dependent maintenance of neural stem cells. Sci. Rep. *8*, 13412.

Origone, P., Verdiani, S., Bandettini, M., Poggio, D., Vignolo, M., Caponnetto, C., Mandich, P., Origone, P., Verdiani, S., Bandettini, M., et al. (2015). A novel Arg147Trp MATR3 missense mutation in a slowly progressive ALS Italian

patient A novel Arg147Trp MATR3 missense mutation in a slowly progressive ALS. Ital. Patient *8421*, 3–5.

Panda, A.C., Martindale, J.L., and Gorospe, M. (2017). Polysome fractionation to analyze mRNA distribution profiles amaresh. Bio Protoc. *7*, e2126.

Potzner, M.R., Tsarovina, K., Binder, E., Penzo-Méndez, A., Lefebvre, V., Rohrer, H., Wegner, M., and Sock, E. (2010). Sequential requirement of Sox4 and Sox11 during development of the sympathetic nervous system. Development *137*, 775–784.

Qiu, C., Ma, Y., Wang, J., Peng, S., and Huang, Y. (2009). Lin28-mediated post-transcriptional regulation of Oct4 expression in human embryonic stem cells. Nucleic Acids Res. *38*, 1240–1248.

Ren, J.I.E., Jian, F., Jiang, H., Sun, Y., Pan, S., and Gu, C. (2018). Decreased expression of SFRP2 promotes development of the pituitary corticotroph adenoma by upregulating Wnt signaling. Int. J. Oncol. *52*, 1934–1946.

Rybak, A., Fuchs, H., Smirnova, L., Brandt, C., Pohl, E.E., Nitsch, R., and Wulczyn, F.G. (2008). A feedback loop comprising lin-28 and let-7 controls pre-let-7 maturation during neural stem-cell commitment. Nat. Cell Biol. *10*, 987–993.

Salton, M., Elkon, R., Borodina, T., Davydov, A., Yaspo, M.-L., Halperin, E., and Shiloh, Y. (2011). Matrin 3 binds and stabilizes mRNA. PLoS One *6*, e23882.

Sarkar, A., and Hochedlinger, K. (2014). The Sox family of transcription factors: versatile regulators of stem and progenitor cell fate. Cell Stem Cell *12*, 15–30.

She, Z.-Y., and Yang, W.-X. (2015). SOX family transcription factors involved in diverse cellular events during development. Eur. J. Cell Biol. *94*, 547–563.

Shi, G., and Jin, Y. (2010). Role of Oct4 in maintaining and regaining stem cell pluripotency. Stem Cell Res. e Ther. 1–9.

Shibayama, M., Ohno, S., Osaka, T., Sakamoto, R., Tokunaga, A., Nakatake, Y., Sato, M., and Yoshida, N. (2009). Polypyrimidine tract-binding protein is essential for early mouse development and embryonic stem cell proliferation. FEBS J. *276*, 6658–6668.

Skowronska-krawczyk, D., Ma, Q., Schwartz, M., Scully, K., Li, W., Kohwi, Y., Kohwi-shigematsu, T., and Rosenfeld, M.G. (2015). HHS public access. Nature *514*, 257–261.

Skowronska-Krawczyk, D., Ma, Q., Schwartz, M., Scully, K., Li, W., Liu, Z., Taylor, H., Tollkuhn, J., Ohgi, K.A., Notani, D., et al. (2014). Required enhancer-matrin-3 network interactions for a homeodomain transcription program. Nature *514*, 257–261.

Tada, M., Doi, H., Koyano, S., Kubota, S., Fukai, R., Hashiguchi, S., Hayashi, N., Kawamoto, Y., Kunii, M., Tanaka, K., et al. (2018). Matrin 3 is a component of neuronal cytoplasmic inclusions of motor neurons in sporadic amyotrophic lateral sclerosis. Am. J. Pathol. *188*, 507–514.

Takahashi, K., and Yamanaka, S. (2016). A decade of transcription factor-mediated reprogramming to pluripotency. Nat. Rev. Mol. Cell Biol. https://doi.org/10.1038/nrm.2016.8.

Temple, S. (2001). The development of neural stem cells. Nature. https://doi.org/10.1038/35102174.

Tenzer, S., Moro, A., Kuharev, J., Francis, A.C., Vidalino, L., Provenzani, A., and Macchi, P. (2013). Proteome-wide characterization of the RNA-binding protein RALY-interactome using the in vivo-biotinylation-pulldown-quant (iBioPQ) approach. J. Proteome Res. *12*, 2869–2884.

Tickle, C., Towers, M., and Davey, M. (2017). Sonic hedgehog signaling in limb development. Front. Cell Dev. Biol. *5*, 1–19.

Vallier, L., Touboul, T., Chng, Z., Brimpari, M., Hannan, N., Millan, E., Smithers, L.E., Trotter, M., Rugg-Gunn, P., Weber, A., and Pedersen, R.A. (2009). Early cell fate decisions of human embryonic stem cells and mouse epiblast stem cells are controlled by the same signalling pathways. PLoS One *4*, e6082.

Wang, X., Zhao, B.S., Roundtree, I.A., Lu, Z., Han, D., Ma, H., Weng, X., Chen, K., Shi, H., and He, C. (2015). N6-methyladenosine modulates messenger RNA translation efficiency. Cell *161*, 1388–1399.

Weed, M., Mundlos, S., and Olsen, B.R. (1997). The role of sonic hedgehog in vertebrate development. Matrix Biol. *16*, 53–58.

Wu, R., Liu, Y., Zhao, Y., Bi, Z., Yao, Y., Liu, Q., Wang, F., Wang, Y., and Wang, X. (2019). m 6 A methylation controls pluripotency of porcine induced pluripotent stem cells by targeting SOCS3/JAK2/STAT3 pathway in a YTHDF1/YTHDF2-orchestrated manner. Cell Death Dis. *10*, 171.

Yamaguchi, A., and Takanashi, K. (2016). FUS interacts with nuclear matrix-associated protein SAFB1 as well as Matrin3 to regulate splicing and ligand-mediated transcription. Sci. Rep. *6*, 1–14.

Yu, J., Vodyanik, M.A., Smuga-Otto, K., Antosiewicz-Bourget, J., Frane, J.L., Tian, S., Nie, J., Jonsdottir, G.A., Ruotti, V., Stewart, R., et al. (2007). Induced pluripotent stem cell lines derived from human somatic cells. Science *318*, 1917–1920.

Yun, S., Leong, C., Zhai, D., Ling, Y., Lim, L., Bi, X., Lee, J., and Jo, H. (2012). Neural stem cell specific fluorescent chemical probe binding to FABP7. PNAS *109*, 10214–10217.

Zeitz, M.J., Malyavantham, K.S., Seifert, B., and Berezney, R. (2009). Matrin 3: Chromosomal distribution and protein interactions. Cell. Biochem. *133*, 125–133.

Zhang, Z., and Carmichael, G.G. (2001). The fate of dsRNA in the Nucleus: a p54nrb-containing complex mediates the nuclear retention of promiscuously A-to-I edited RNAs. Cell *106*, 465–475.

Zhuang, M., Li, X., Zhu, J., Zhang, J., Niu, F., Liang, F., Chen, M., Li, D., Han, P., and Ji, S. (2019). The m 6 A reader YTHDF1 regulates axon guidance through translational control of Robo3 . 1 expression. Nucleid Acids Res. *47*, 4765–4777.

iScience, Volume *24*

Supplemental information

Multilayer and MATR3-dependent regulation of mRNAs maintains pluripotency in human induced pluripotent stem cells

Daniele Pollini, Rosa Loffredo, Federica Maniscalco, Marina Cardano, Mariachiara Micaelli, Isabelle Bonomo, Nausicaa Valentina Licata, Daniele Peroni, Weronika Tomaszewska, Annalisa Rossi, Valeria Crippa, Erik Dassi, Gabriella Viero, Alessandro Quattrone, Angelo Poletti, Luciano Conti, and Alessandro Provenzani

SUPPLEMENTARY FIGURES AND TRANSPARENT METHODS

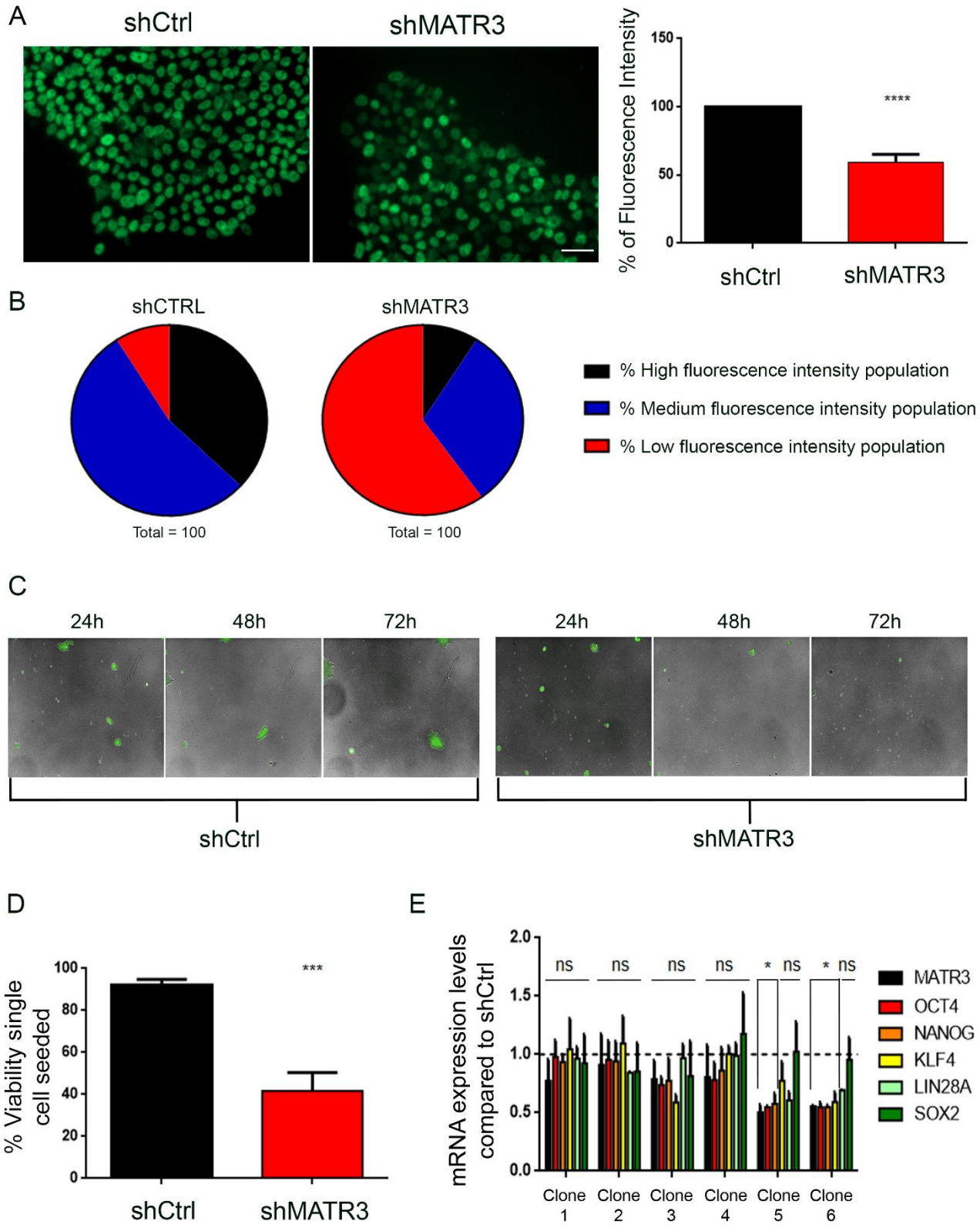

Figure S1. MATR3 is essential for the clonogenic ability of human iPSCs. Related to figure 1

(A) Representative picture of MATR3 immunofluorescence staining (Scale bar: 50 µm). The quantification of immunofluorescence intensity was performed using the ImageJ intensity measurement of the nucleus area. Data are reported as mean ± S.E.M. for four replicates, t-test (*** P<0.001). **(B)** The single-cell fluorescence quantification allows

the classification into three different cell subpopulations present in shCtrl and shMATR3 cell lines, a low-intensity fluorescence population (≤ 200000 arbitrary units (a.u.) 70% of mean fluorescence intensity in shCtrl population), medium (from 200000 a.u. to 300000 a.u.) and a high fluorescence intensity cell population (≥ 300000 a.u.). The mean fluorescence intensity in shCtrl population reported was 280000 a.u., while the mean of fluorescence intensity reported in shMATR3 population was 195065 a.u. **(C)** Alkaline Phosphatase (AP) assay performed on shCtrl and shMATR3 cell line single cell. The images were acquired with the Operetta High Content Screening System (Perkin Elmer) using 2X objective 0.08NA. Colonies are reported for each time point. **(D)** Limiting dilution assay, the percentage of wells in which colonies developed after single cell plating. Data are reported as mean ± S.E.M. for three replicates, t-test (*** $P<0.001$). **(E)** RT-qPCR analyses for *MATR3, OCT4, NANOG, KLF4, LIN28A* and *SOX2* on shMATR3 colonies derived from single-cell seeding (on 6 clones). RT-qPCR analyses were normalized on internal housekeeping (*β-ACTIN*) and reported in comparison to shCtrl values (reported as value 1 in the graph). Values, are reported as mean ± S.E.M. P-value, was calculated by Two-way ANOVA (* $P<0.05$).

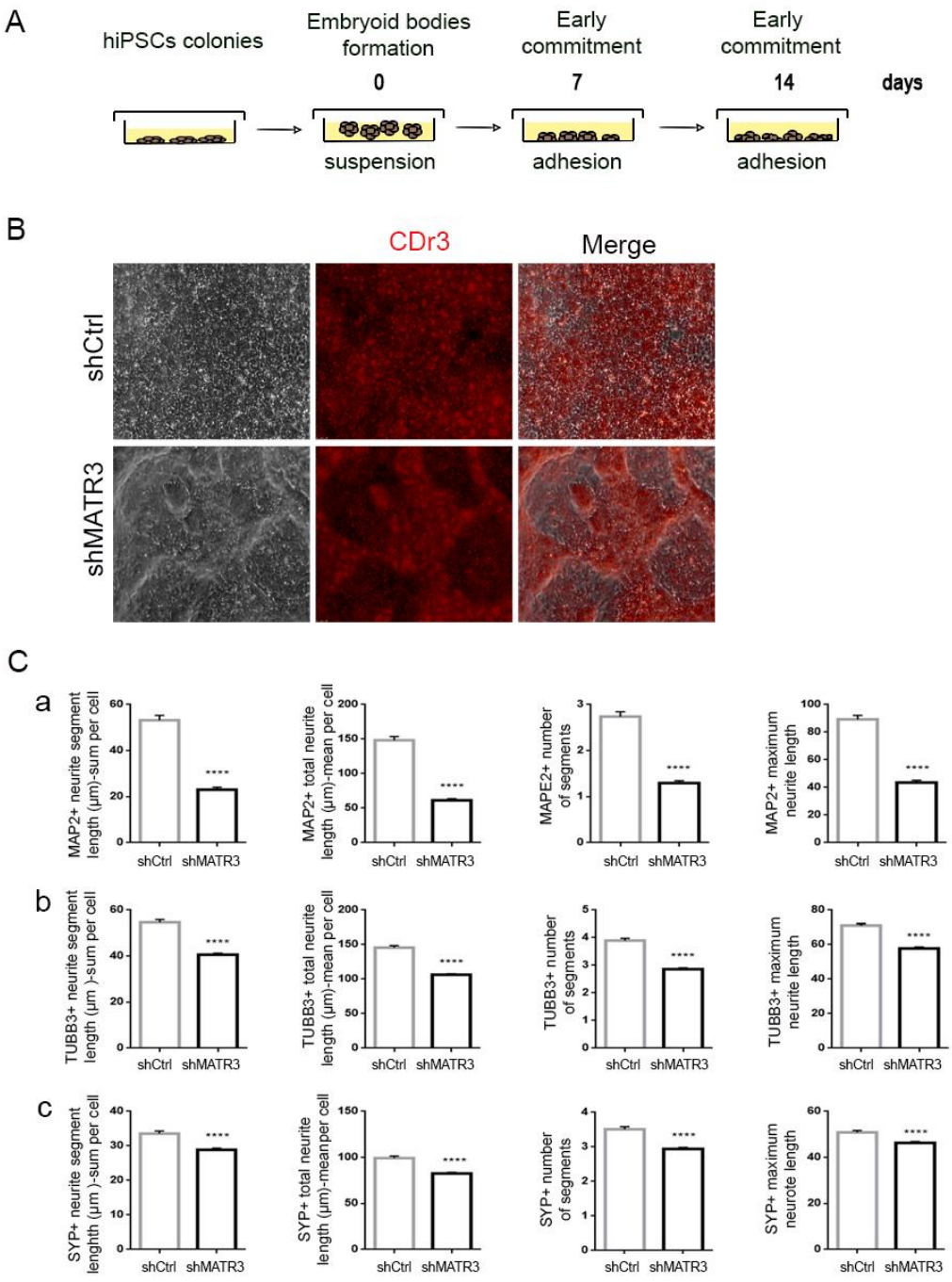

Figure S2. MATR3 is required for hiPSCs neuronal differentiation. Related to figure 2

(A) Schematic diagram of the protocol for EB assay. hiPSCs were dissociated and plated in suspension cultures for 7 days and then replated on Geltrex-coated culture plastic for an additional seven days. **(B)** Differentiation into Neural progenitors was confirmed by staining for NeuroFluor CDr3. **(C)** Morphometric neurite analyses on MNs from shMATR3 and control at day 53 of terminal differentiation. The sum per cell or the mean per cell of neurite segments (µm), the number of cell neurites and the maximum neurite length (µm) of neuronal cells labelled with MAP2 (**a**), TUBB3 (**b**) and SYP (**c**) were measured with Columbus software. Data were obtained by single-cell immunofluorescence analyses (**** *P*<0.0001).

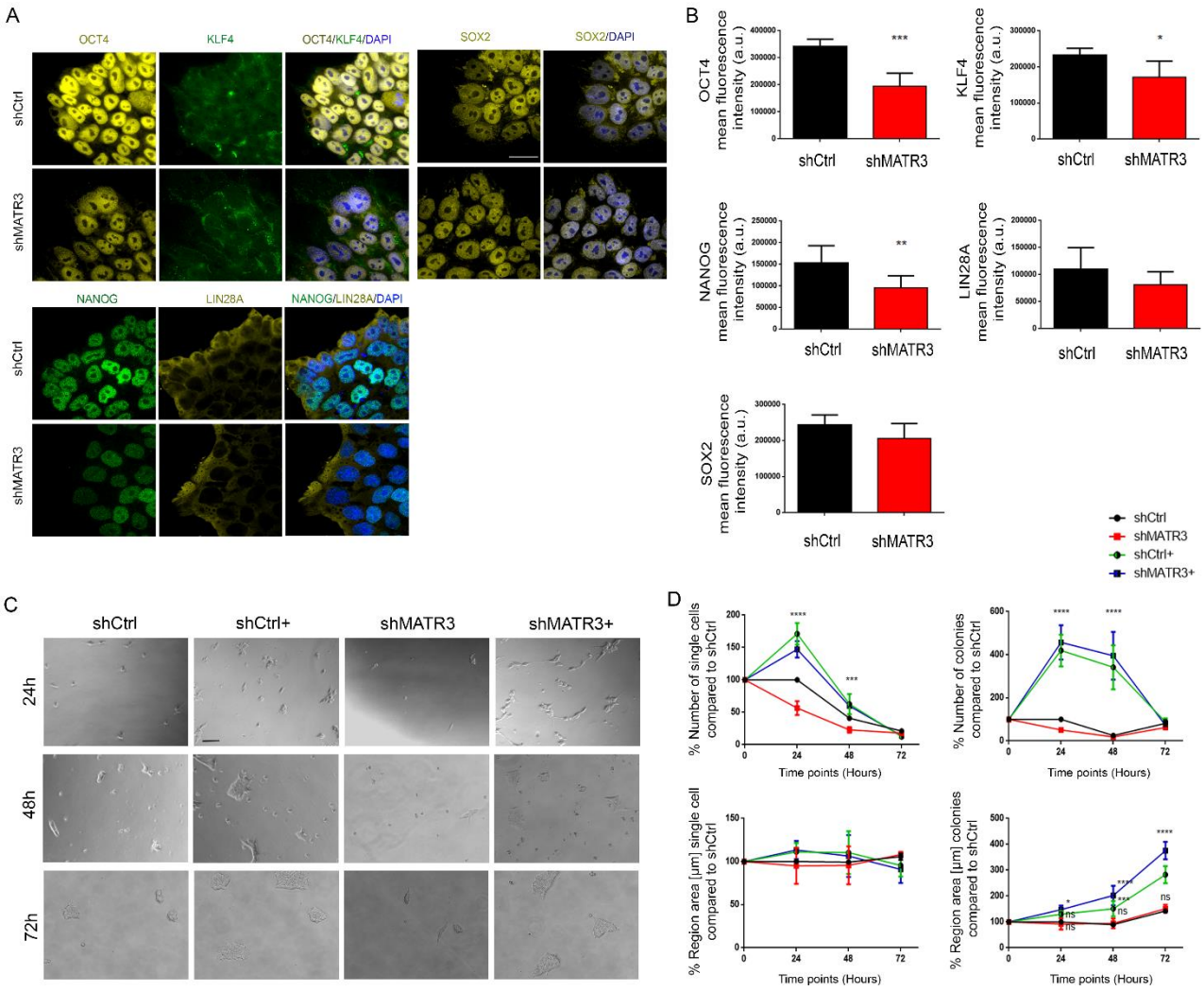

Figure S3. MATR3 downregulation decreases the expression level of OCT4, NANOG, KLF4 and *LIN28A*. Related to figure 3

(A) Immunofluorescence staining for pluripotency markers OCT4, KLF4, NANOG, LIN28A, and SOX2. Cell nuclei were stained with DAPI in blue (Scale bar: 25µm). **(B)** The quantification of immunofluorescence intensity was performed using the ImageJ mean fluorescence intensity measurement. Data are reported as mean ± S.E.M. for nine replicates from 3 different biological replicates; *P*-value was calculated using *t-test* (*ns*, not significant; * *P*<0.05; ** *P*<0.01; *** *P*<0.001). **(C)** Pictures of shCtrl, shCtrl+, and shMATR3, shMATR3+ in three different time points (24, 48, and 72 hours). Cells were seeded in single cells and small colonies (sub-optimal condition), with and without the overexpression of MATR3 wt. Scale bar 100 µm. **(D)** Cell growing quantification of shCtrl, shCtrl+ and shMATR3 shMATR3+ hiPSCs in sub-optimal condition. Images were acquired with the Operetta High Content Screening System using 2X objective 0.08NA (data not shows). The region Areas [µm] for the single cells and the colonies are reported for each time point. Two-way ANOVA (** *P*<0.01; *** *P*<0.001).

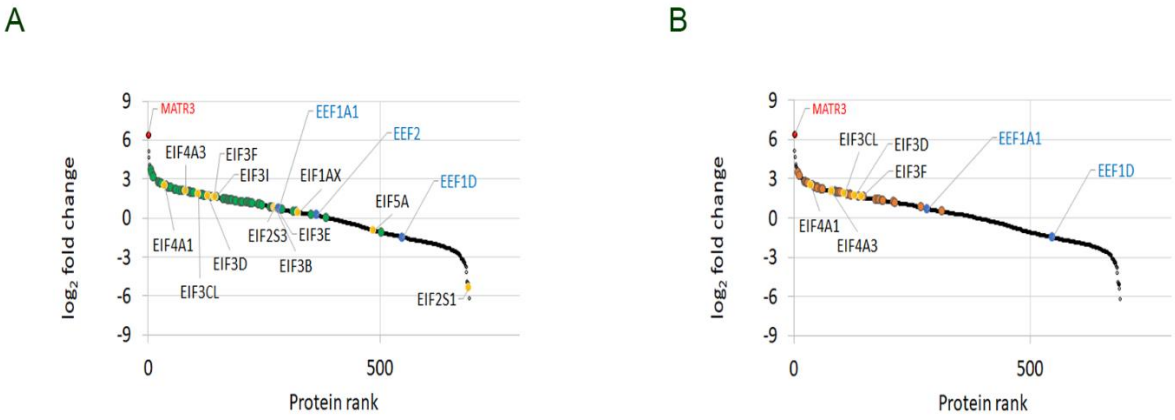

Figure S4. MATR3 is associated with the translation machinery and RNA processing. Related to figure 4, tables S1, S2 and S3

(A) Protein ranking based on log2 fold-changes (MATR3/ IgG) for all the proteins identified by MS. **(B)** Protein ranking based on log2 fold-changes (MATR3/IgG) for the proteins significantly enriched in MATR3 pulldowns (*P*-val < 0.05). Each data point represents a singles protein. Colour code: green dots, ribosomal proteins; yellow dots, Eukaryotic Initial factor (EIF) proteins; blue dots indicate the Eukaryotic elongated factors (EEF) proteins. In red, MATR3 protein.

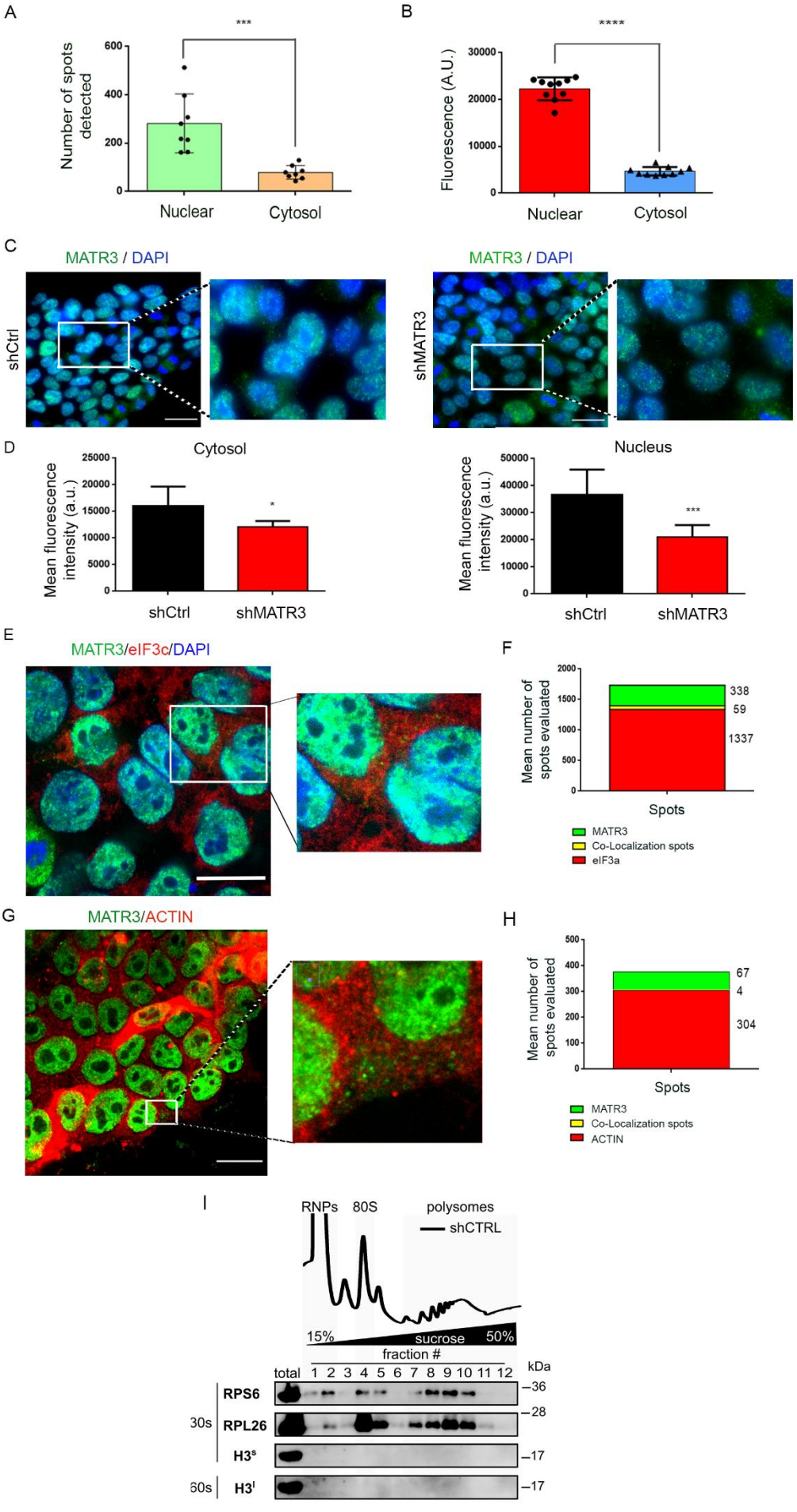
A
***
Number of spots detected
600
400
200
0
Nuclear
Cytosol
B
****
Fluorescence (A.U.)
30000
20000
10000
0
Nuclear
Cytosol
C
MATR3 / DAPI
shCtrl
MATR3 / DAPI
shMATR3
D
Cytosol
Mean fluorescence intensity (a.u.)
25000
20000
15000
10000
5000
0
*
shCtrl
shMATR3
Nucleus
Mean fluorescence intensity (a.u.)
50000
40000
30000
20000
10000
0
***
shCtrl
shMATR3
E
MATR3/eIF3c/DAPI
F
Mean number of spots evaluated
2000
1500
1000
500
0
338
59
1337
Spots
MATR3
Co-Localization spots
eIF3a
G
MATR3/ACTIN
H
Mean number of spots evaluated
500
400
300
200
100
0
67
4
304
Spots
MATR3
Co-Localization spots
ACTIN
I
RNPs
80S
polysomes
shCTRL
15%
sucrose
50%
fraction #
total
1 2 3 4 5 6 7 8 9 10 11 12
kDa
RPS6
RPL26
H3s
H3l
30s
60s
36
28
17
17

Figure S5. MATR3 regulates the translation efficiency of LIN28A, NANOG and SOX2 mRNAs. Related to figure 5

(A) Graph reporting the immunofluorescence analysis of MATR3 subcellular localization in hiPSCs. Quantification of immunoreactive spots in the cytoplasm and inside the nucleus is reported. The analysis was performed using the ImageJ "Find maxima" plug-in. Data are reported as mean ± S.E.M. for eight replicates. *P*-value was calculated using *t-test* (*** *P*<0.001). **(B)** Histogram indicating the nuclear and cytosplasmic fluorescence mean intensity. The analysis was performed using the ImageJ "Find maxima" plug-in. Data are reported as mean ± S.E.M. for eight replicates. *P-value* was calculated using *t-test* (**** *P*<0.0001). **(C)** Immunofluorescence staining for MATR3. The enlargement highlights the MATR3 spots outside the nucleus in shCtrl and shMATR3 cell lines(I). Cell nuclei were stained with DAPI in blue (Scale bar: 25µm). **(D)** Histograms reporting the different fluorescence intensity quantified by the ImageJ "Find maxima" plug-in. In the left was reported the cytosol MATR3 fluorescence intensity and in the right the MATR3 nucleus fluorescence intensity. In both cases, the fluorescence intensity calculated was compared between the shCtrl and shMATR3 cell lines. Data are presented as the mean ± S.E.M. *P-value* was calculated using *t-test* (* P<0.05; *** *P*<0.001). **(E)** Pictures of hiPSCs stained for MATR3 (green signal) and eIF3c (red signal). Scale bar 20 µm. **(F)** eIF3a and MATR3 co-localization analysis on 3D (x,y,z) immunofluorescent single cells images; only cytoplasm area of each cell was considered. The histogram staked bars graph reported data obtained by six replicates (two biological replicates). 20% of total spots of MATR3 co-localize with eIF3a, where the 4% of total spots of eIF3a co-localized with MATR3. **(G)** Pictures of hiPSCs stained for MATR3 (green signal) and β-ACTIN (red signal) a negative control. Scale bar 20 µm. **(H)** β-ACTIN and MATR3 co-localization analysis on 3D (x,y,z) immunofluorescent single cells images; only cytoplasm area of each cell was considered. The histogram staked bars graph reported data obtained by six replicates (two biological replicates). 5% of total spots of MATR3 co-localize with β-ACTIN, where the 1% of total spots of βACTIN co-localized with MATR3. **(I)** Polysome profiling of shCtrl hiPSCs and western blotting images on proteins extracted from total cell lysate and proteins extracted from sucrose gradient fractions. H3 is used as nuclear marker and RPS6 and RPL26 as ribosomal markers. The signal of H3 along the profile is shown for short ($H3^{s}$) and long ($H3^{l}$) times of acquisition. RSP6, RPL26 and $H3^{s}$ are acquired at the same exposition time (30s). $H3^{l}$ is acquired at longer time (60s) to confirm the absence of signal along the profile.

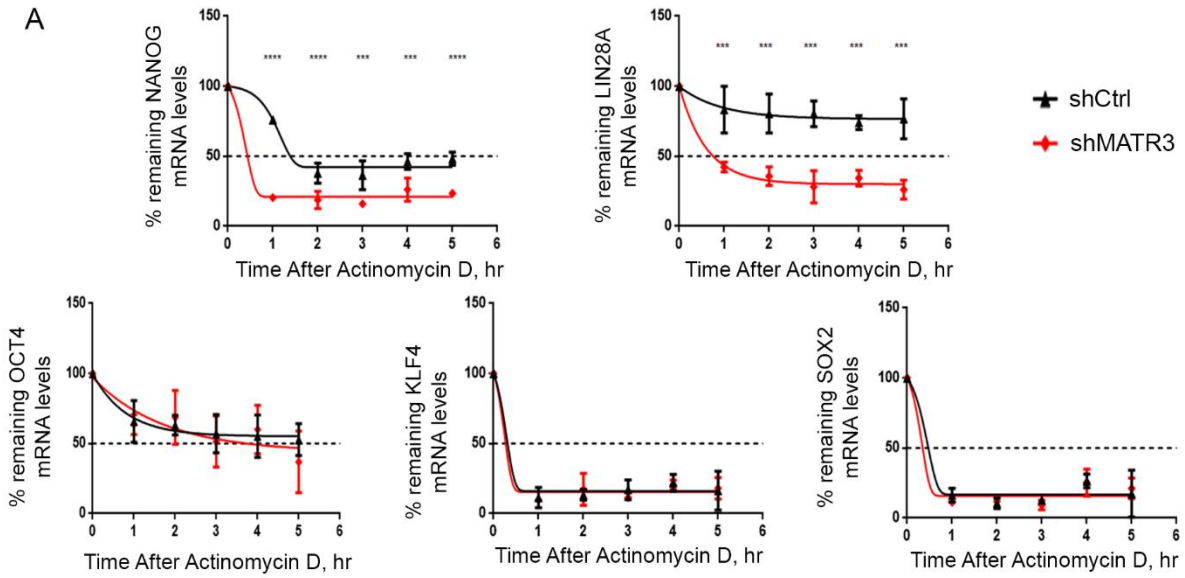

Figure S6. MATR3 stabilizes *NANOG* and *LIN28A* mRNAs. Related to figure 6

(A) qRT-PCR analysis for the evaluation of mRNA half-lives in shCtrl and shMATR3 hiPSCs performed by Actinomycin-D assay. qRT-PCR values are normalized to their internal housekeeping (β-ACTIN). Results are expressed as percentages of mRNA abundance relative to Time 0. Statistical analysis was performed on the mean of three biological replicates, two-way ANOVA (*** *P*<0.001; **** *P*<0.0001).

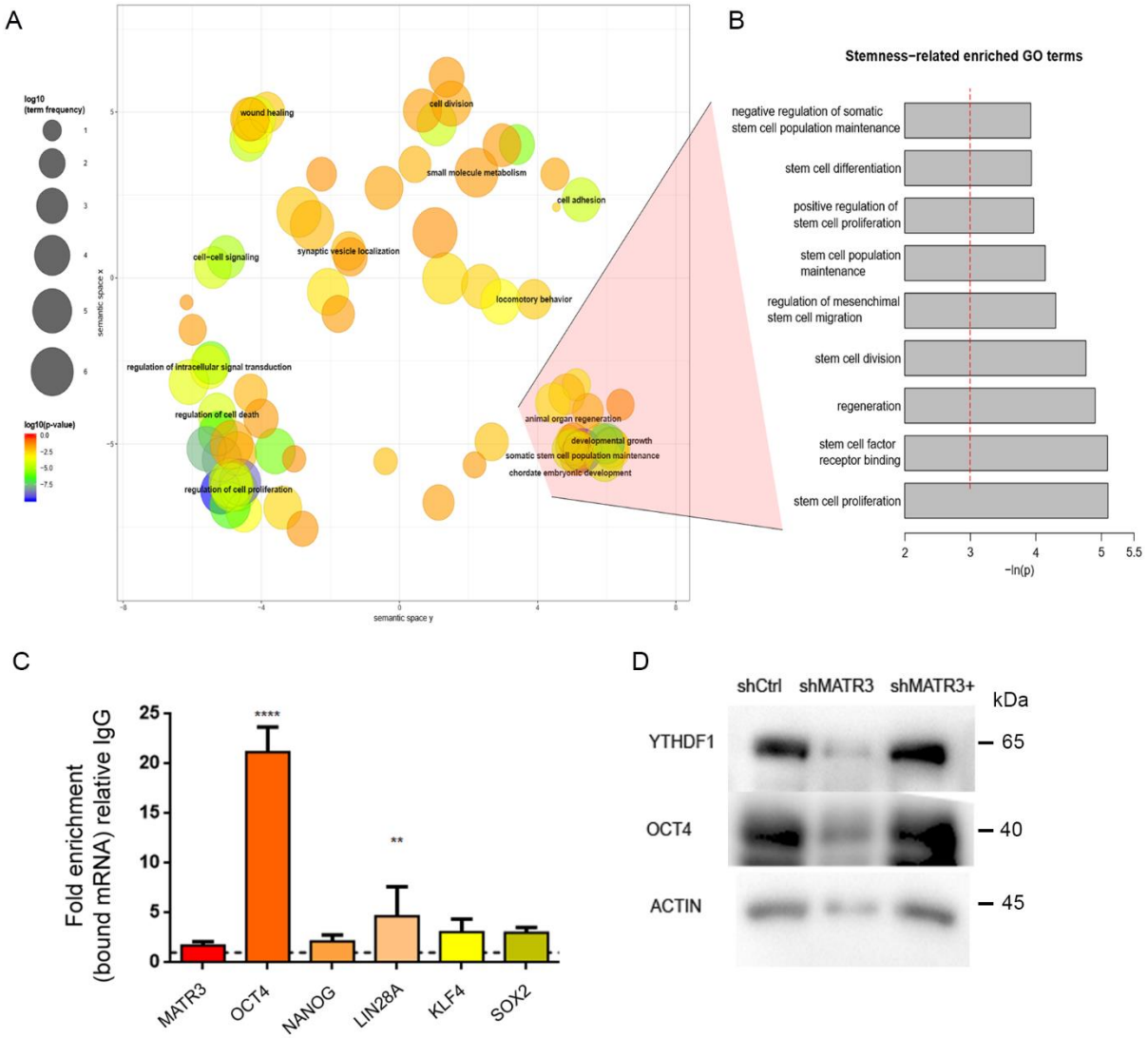

Figure S7. MATR3 binds development gene promoters and sustains OCT4 expression by regulating *YTHDF1* expression. Related to figure 7, tables S4 and S5

(A) Semantic similarity of enriched Gene Ontology terms (biological process branch). Functionally related processes are close to one another, with circle size representing the abundance of genes annotated to that process in the genome. The colour gradient represents the enrichment P-value. (Supp Table 4) **(B)** Barplot of significantly enriched Gene Ontology terms related to stemness processes, *P*-values are expressed in -log10(*P*-value) and the red line indicates the adjusted *P*-value threshold (0.05). **(C)** RIP using m6A antibody in the Gibco cell line (A18945), followed by RT-qPCR. Fold enrichment was relative to IgG. Represented graphically as the mean ± S.E.M. of three biological replicates. One-way ANOVA (** *P*<0.01; **** *P*<0.0001). **(D)** Single Western Blot analysis showed the overexpression of YTHDF1. Analyses for YTHDF1, OCT4 and ACTIN, was performed on shCtrl-, shMATR3-, and YTHDF1 overexpressed in shMATR3- (+) cultures.

EXPERIMENTAL PROCEDURES

Cell Culture and generation of stable cell line

Human Episomal Pluripotent Stem Cell (hiPSC) line (Gibco, A18945) was cultivated on Geltrex (Thermo Fisher Scientific) coated plates in TeSR-E8 Medium (STEMCELL) according to the manufacturer's indications. Cultures were passaged by using 0.5 mM EDTA as detaching agent. To establish the MATR3-silenced line, cells were infected with MATR3 shRNA, targeting MATR3 3'UTR, or control shRNA lentivirus (MISSION shRNA NM_018834 and PLKO.1-puro respectively, Sigma-Aldrich) and selected with 1µg/mL puromycin. Lentiviral particles were generated in HEK293T cells by co-transfecting the Δ891 and VSV-G encoding vectors along with the shRNA transfer lentiviral plasmid PLKO and shMATR3 plasmid. shCtrl and shMATR3 have been subject of molecular analysis (every two weeks) to check and confirm the appropriate level of MATR3 downregulation. To establish the GFP expression under *OCT4* promoter in hiPSCs line (Gibco, A18945), cells were infected with Human Oct-4 Differentiation Reporter (pGreenZeo, plasmid) (SBI cat #SR10033PA-1). To establish the MATR3-silenced on hiPSCs/OCT4-GFP line, cells were infected with MATR3 shRNA or control shRNA lentivirus (MISSION shRNA NM_018834 and PLKO.1-puro respectively, Sigma-Aldrich) and selected with 1µg/mL puromycin.

Cell assays

Viability assay was performed on cells cultured for 96h. Every 24h, OZBlue assay (OZbiosciences) was performed by incubating the plates at 37°C for 4h following the manufacturer's protocol. Absorbance was detected at 570nm by Infinite M200 (Tecan) plate reader. Cell proliferation of hiPSCs was measured using a Click-iT EdU Imaging Kit (Thermo Fisher Scientific) according to the manufacture's indications. For EdU incorporation, cells were labelled by incubation with 1µM EdU for 2h at 37°C. Labelled cells were immediately fixed with 3.7% formaldehyde in PBS and permeabilized by 0.5% Triton X-100 for 30 min at RT, followed by EdU detection using 10µM Alexa Fluor-488 for 45 min at RT. Standard flow cytometry method was used then to determine the percentage of S-phase cells in the population. Alkaline Phosphatase Live Stain (AP) (Thermo Fisher Scientific), was assessed following the manufacturer's protocol by incubating cell cultures at 37°C for 30 min. Images were acquired with the Operetta High Content Screening System (Perkin Elmer) using 2X objective 0.08NA and analysed using the software Harmony 4.1 (Perkin Elmer). The number of cell colonies and the number of single cells were counted, and the intensity of the fluorescent signal was measured for both populations. Rescue experiments were done by nucleofecting hiPSCs (Lonza Amaxa 4D-Nucleofector; the program used P3 Nucleofector Sample, CB-150) with the pCMV6-AN-His-HA-MATR3 plasmid in the shMATR3 cell line. After the plasmid's nucleofection with MATR3 wt plasmid, the cells were seeded in StemFlex media (Thermo Fisher Scientific) and 10 µg/ml of Y-27632 ROCK inhibitor (MACS, Miltenyi Biotec) for one day. After 24 hours, the media was changed with the new one and left growing for 48h before collecting the pellet for RT-qPCR and WB analysis. Limiting diluition experiment was performed by plating shCtrl and shMATR3 single cell in 96 well. To support the attachment and growth of the single-cell was used the Gibco StemFlex media and 10 µg/ml of Y-27632 ROCK inhibitor (MACS, Miltenyi Biotec) for one day.

EB formation and morphometric parameters

EBs assay was performed by plating hiPSC clumps in ultralow attachment plates (Voden) in TeSR-E8 Medium supplemented with 2 mg/mL of PVA (polyvinyl alcohol, Sigma-Aldrich) and 10 µg/ml of Y-27632 ROCK inhibitor (MACS, Miltenyi Biotec) for one day. Then, cell aggregates were shifted to a 1:1 mix of Essential 6 medium (E6 medium, Thermo Fisher Scientific) and TeSR-E8 Medium supplemented with 2 mg/mL of PVA for

two days. After two days, the medium was replaced with Essential 6 medium. After one week, Embryoid Bodies were collected and plated on Geltrex-coated plastic 6-well plates and let to differentiate for further 7 days in Essential 6 medium. The medium was renewed entirely every other day. Brightfield cultures' images were captured with a Leica DM IL LED microscope equipped with a DFC450C digital camera (Leica Microsystem). EBs Images were also acquired with the Operetta High Content Screening System (Perkin Elmer) using 2X objective 0.08NA, and EBs count and morphometric properties were calculated using the software Harmony 4.1 (Perkin Elmer). Elongation distortion index (EDI) expressed the extent of axial elongation and was calculated as (1/[circularity]-1) using ImageJ software, as previously reported (Warkus *et al.*, 2016).

Neuronal differentiation

Motor neuron differentiation was performed as previously described (Jha et al., 2015). Briefly, hiPSCs were seeded on Geltrex-coated 6-well plate in TeSR-E8 Medium supplemented with 10 µM Y27632. The following day, cells were exposed to PSC Neuronal Induction Medium (NIM, Thermo Fisher Scientific). At day 7, cultures were dissociated and replated in NIM supplemented with 10 µM Y27632. The following day, the medium was replaced by the fresh medium without Y27632. From day 10, the presence of Neural Progenitors cells (NPCs) was checked by live membrane-permeable fluorescent probe NeuroFluor CDr3 (STEMCELL). When NPCs reached the 80% of confluence, the medium was shifted to StemPro ESC SFM (Thermo Fisher Scientific) supplemented with 1µM Purmorphamin (Pur) (MACS, MilenyiBiotec), 50µM Retinoic Acid (RA) (Sigma-Aldrich), 8 ng/mL FGF-2 (Voden) and 10 ng/mL Activin (Voden). At 100% confluency, cultures dissociated by using Accutase (Thermo Fisher Scientific) and replated on polyornthine/laminin coated plastic in StemProhESC SFM medium supplemented with 10 ng/mL BDNF (Miltenyi Biotec) and 10 ng/mL GDNF (Voden). The medium was replaced every other day.

Cell extracts and Western Blot Analysis

Samples were lysed in RIPA lysis buffer supplemented with Protease Inhibitor Cocktail (Thermo Scientific). Equal amounts of proteins were separated on 10% SDS-PAGE and blotted onto PVDF membrane (GE Healthcare). Primary and secondary antibodies used are reported in Table2. The immunoreactive signals were detected by incubation with Amersham ECL Selected (GE) and acquisition with the Chemidoc Imaging System (BioRad).

RNA extraction and real-time PCR

Total RNA was extracted by Trizol Reagent (Thermo Fisher Scientific) according to the manufacturer's protocol and then retro-transcribed with RevertAid RT Reverse Transcription Kit (Thermo Fisher Scientific). cDNAs were used to verify the expression of specific target genes by RT-PCR (primer sequences are reported in Table3) by using the KAPA SYBR FAST qPCR Master Mix (2X) kit (Kapa Biosystems) according to the manufacturer's specifications. qRT-PCR data were analysed according to the comparative ΔΔCt method and normalized by using β-ACTIN housekeeping gene.

Immunocytochemistry and fluorescence microscopy

Cultures were gently washed in pre-warmed PBS and then fixed in 4% PFA (Sigma-Aldrich) in PBS pH 7.4 for 15 min at room temperature, permeabilized with 0.3% Triton X-100 in PBS for 10 min, and then incubated in blocking solution (PBS, 5% FBS, 0.2% Triton X-100) for 90 min. Incubation with primary antibodies was performed overnight at 4°C in antibody solution (Ab dilutions indicated in Table2). Incubation with the appropriate Alexa Fluor secondary antibodies (Thermo Fisher Scientific) was performed at room temperature

for 1h followed by nuclei were counterstained with 1 µg/ml Hoechst 33258 or DAPI (Thermo Fisher Scientific) for 10 min at room temperature. Fluorescent signals were acquired using different instruments: i) Leica DM IL Led Fluo microscope and Leica DFC450 C (Leica Microsystem) camera, ii) Operetta High Content Screening System (PerkinElmer) using 20x 0.75NA and 40x 0.95NA objectives, iii) Zeiss Axio Observer Z1 equipped with Colibri 1, ApoTome 1 and Cell Observer modules, iv) Nikon Eclipse Ti2-E equipped with spinning disc unit and VCS. Neural rosettes analysis was carried out by plating $1.8*10^4$ NPCs in CellCarrier-96 Black plate (PerkinElmer). Rosettes and neurites outgrowth was calculated by analysing the images with Columbus 3.5.2 software (PerkinElmer). MAP-2/βIII-TUBULIN/SYNAPTHOSIN-positive cells were selected and analysed for neurites morphology by using the neurite tracing algorithm (CSIRO Neurite Analysis). Localization, fluorescence intensity and co-localization analysis were performed by ImageJ Fiji software. The count of MATR3 green-positive dots and their fluorescence quantification in the nuclear and cytoplasmic regions was performed by using the ImageJ "Find maxima" plug-in, on maximum intensity projection. Images' pre-processing before the dots count analysis only involved uniform denoising and background subtraction steps. The total number of nuclear or cytoplasmic dots was then divided by the number of nuclei present in each field of view. The colocalization analysis between eIF3A and MATR3 was performed on 3D (x,y,z) images of single cells, considering only the cytoplasmic area of each cell. Images' pre-processing before colocalization analysis only involved uniform denoising and background subtraction steps. The total number of eLF3A and MATR3 dots, as well as the total number of MATR3 dots touching eLF3A dots, was evaluated by using the ImageJ "DiAna v.1.47" plug-in (Gilles et al., 2017). DiAna plug-in settings were optimized for successful detection and segmentation of the spot-like structures corresponding to eLF3A or MATR3 fluorescent signals and were kept constant for all the analysed images.

Immunoprecipitation assay and Mass Spectrometry analyses

Immunoprecipitation (IP) was performed as previously described (Bonifacino, Gershlick and Angelica, 2016). Briefly, hiPSCs were lysed in Lysis Buffer (20 mM Tris–HCl at pH 7.5, 100 mM KCl, 5 mMMgCl2 and 0.5% NP-40) and subjected to IP by using anti-MATR3 IgG-IP control with a mixture of Dynabeads Protein A and protein G (Thermo Fisher). These were incubated with MATR3 antibodies or mouse IgG at 4°C for 1h, and then incubated with lysate overnight at 4°C. Beads were washed three times with washing buffer (0.05% Tween20 and 50 mM ammonium bicarbonate pH 8) and additional three times with 50 mM ammonium bicarbonate, to remove any residual detergent. Bound protein complexes were eluted with urea buffer (8M Urea, 100 mM ammonium bicarbonate pH 8), reduced using 10 mM DTT for 1 hour and alkylated with 20 mM iodoacetamide (IAA) in the dark for 30 minutes at room temperature. Subsequently, the proteins were digested with 0.5 µg Lys-C (Promega) for 4h and then diluted in 50mM ammonium bicarbonate in water before being further digested with 1 µg trypsin overnight at room temperature. Resulting peptide solution was desalted on C18 stage-tips and vacuum dried before being resuspended in 20 µl of 0.1% formic acid buffer for LC-MS/MS analysis. Samples were analyzed using an Easy-nLC 1200 system coupled online with an Orbitrap Fusion Tribrid mass spectrometer (both Thermo Fisher Scientific, San Jose, CA, USA). A reversed-phase column (Thermo Fisher Scientific, Acclaim PepMap RSLC C18 column, 2µm particle size, 100Å pore size, id 75 µm) with a two-component mobile phase system of 0.1% formic acid in water (buffer A) and 0.1% formic acid in acetonitrile (buffer B) was used for separating the digested peptides. Peptides were eluted using a gradient of 5% to 25% over 52 minutes, followed by 25% to 40% over 8 minutes and 40% to 98% over 10 minutes at a flow rate of 400 nL/min. The data-dependent acquisition (DDA) method is based on full scans performed at 120.000 fwhm resolving power (at 200 m/z) and an AGC target of $1x10^6$. Full scans were followed by a set of (HCD) MS/MS scans over 3 sec cycle time, at a collision energy of 30%, 150 ms of maximum injection time (ion trap) and AGC target of $5x10^3$. A mass range of 350-1100 m/z was surveyed for precursors, with first

mass set at 140 m/z for fragments. The DDA data files were searched in Proteome Discoverer 2.2 software (Thermo Fisher Scientific). Peptides searches were performed using Human protein FASTA file (UniProt, reviewed, downloaded July 2019). Proteins were identified using the SEQUEST HT search engine using precursor mass tolerance of 10 ppm and product mass tolerance of 0.6 Da. Trypsin was chosen as the enzyme with 3 missed cleavages, and static modification of carbamidomethyl (C) with variable modification of oxidation (M) was incorporated in the search. PSMs and protein false discovery rate were filtered for <0.01. Peak intensities were log2 transformed and data were normalized by the average of the protein abundance with each sample (Aguilan et al., 2020). Statistical significance was assessed using Student's t test (two-tailed, two-sample unequal variance). Functional enrichment *and* interaction network analyses were performed on the proteins that were at least 1.5-fold enriched in MATR3 IP versus IgG ($p \leq 0.05$). Gene Ontology enrichment analysis was conducted using FunRich software, version 3.1.3 (http://www.funrich.org) (Pathan *et al.*, 2015). Protein-protein *interaction network was* constructed using STRING interaction database, version 11.0 (https://string-db.org/) (von Mering et al., 2003). Only high confidence interactions (score > 0.7), as determined by the STRING database, were accepted.

RNA Immunoprecipitation Assay

RNA Immunoprecipitation (RIP) assay was performed as previously described (Keene et al., 2006). Briefly, 1,2 x 10^7 hiPSCs were lysed in 20 mM Tris–HCl at pH 7.5, 100 mM KCl, 5 mM $MgCl_2$, and 0.5% NP-40 for 10 min on ice and centrifuged at 15 000 × g for 10 min at 4°C. A mixture of Dynabeads Protein A and protein G (Thermo Fisher) were incubated with YTHDF1 or MATR3 antibodies or normal IgG at 4°C for 1h, and then incubated with lysate overnight at 4°C. The beads were washed with NT2 buffer (50 mM Tris–HCl pH 7.5, 150 mM NaCl, 1 mM $MgCl_2$, 0.05% NP-40). RNA was purified from the supernatant using TRIzol Reagent following the procedure described before and used for RT-qPCR validation.

ChIP-seq analysis and ChIP

Bedgraph-format data were obtained from GEO with ID GSM1399416 (Skowronska-Krawczyk et al., 2014), and peaks were called with MACS2 (Zhang *et al.*, 2008), using the *bdgpeakcall* command with default parameters. HOMER (Heinz et al., 2010) was then used to annotate the closest gene to each peak (*annotatePeaks* command) and to detect consensus motifs (*find Motifs* command with scrambled input sequences obtained with the *scramble Fasta* command as background) from the 100 nucleotides surrounding the peak centre of the 500 most significant peaks obtained, ranked by their peak score (-10*log10p-value). The two most significant motifs, as ranked by their p-value, were retained. Gene Ontology enrichment analysis was performed with HOMER (Heinz et al., 2010) (*annotatePeaks* command with *-go* option) on all three branches (BP, MF, CC), using a 0.05 threshold on Benjamini-Hochberg adjusted p-value. The Gene Ontology enrichment results were plotted with REVIGO (Supek et al., 2011) (XY plot with 0.7 similarity threshold). Chromatin Immunoprecipitation (ChIP) was performed as described previously (Thongon et al., 2016).

Click-it and Polysome analysis

The global protein synthesis was evaluated by the Click-iT Plus OPP Alexa Fluor Protein Synthesis Assay Kit (Thermo Fisher), according to the manufacturer's specifications. Polysome analysis was performed as described in (Panda et al., 2017). Briefly, shCtrl and shMATR3 cell lines were grown on 10 cm Petri dishes with TeSR-E8 medium. Cells were incubated in medium supplemented with cycloheximide (0.1 mg/ml) for 10 min. Then cells were washed three times with cold PBS plus cycloheximide (0.1 mg/ml) and lysed with the lysis buffer (100 mM NaCl, 5 mM $MgCl_2$, 20 mM Tris–HCl pH 7.5, 0,5% Nonidet P-40, 100 U/ml of RNase inhibitors from human placenta (NEB), 1 mM DTT, 0.1 mg/ml cycloheximide, proteinase inhibitor mixture

(Roche)). The lysate was centrifuged at 14000 g for 5 min and 4°C to obtain a nuclei and mitochondria free supernatant, which was loaded on 15%-50% sucrose gradients (2.2 M Sucrose, H_2O, 10X salts solution (1000mM NaCl, 200mM Tris-HCL, 50mM $MgCl_2$)). Supernatant were ultracentrifuged in a SW41 rotor for 1h and 40 min at 4°C and 40000 rpm in a Beckmann Optima ultracentrifuge. The sedimentation profiles were monitored by absorbance at 254 nm using an ISCO UA-6 UV detector, and 1 ml of each fraction was collected. For Western blot analysis, proteins were extracted using the methanol/chloroform extraction as in (Lauria et al., 2020). Protein pellets were solubilized directly in pH 8.0 Laemmli buffer. mRNA co-sedimentation: RNA from each sucrose fraction was extracted using Trizol or phenol–chloroform as described previously (Lauria et al., 2020; Tebaldi et al., 2012), Equal volumes of RNA were used for cDNA synthesis using the RevertAid RT Reverse Transcription Kit (Thermo Fisher Scientific). cDNAs were used to verify the expression of specific target genes by RT-PCR (primer sequences are reported in Table3) by using the KAPA SYBR FAST qPCR Master Mix (2X) kit (Kapa Biosystems) according to the manufacturer's specifications.

mRNA stability analysis

The mRNA stability analysis was performed to determinate mRNA half-life in shMATR3 and shCtrl cultures. Cells were treated with 5 μg/mL of Actinomycin D (Thermo Fisher) for 1 to 5h. After RNA extraction, described previously, an RT-qPCR was performed with β-ACTIN used as housekeeping to normalize. The results are expressed as percentages of mRNA abundance relative to time 0.

Statistical analysis

All statistical analyses were performed using GraphPad Prism 6 software (GraphPad Software Inc.). Tested used were: One-way ANOVA, Two-way ANOVA and t-test. Data were presented as mean ± standard deviation (SD) or statistical error of the mean (SEM), as indicated for the specific experiment, indicated in the figure legend, $P<0.05$ was considered statistically significant.

References

Aguilan, J.T., Kulej, K., Sidoli, S., 2020. Guide for protein fold change and p -value calculation for non-experts in proteomics . Mol. Omi.

Gilles, J.F., Dos Santos, M., Boudier, T., Bolte, S., Heck, N., 2017. DiAna, an ImageJ tool for object-based 3D co-localization and distance analysis. Methods 115, 55–64.

Heinz, S., Benner, C., Spann, N., Bertolino, E., Lin, Y.C., Laslo, P., Cheng, J.X., Murre, C., Singh, H., Glass, C.K., 2010. Simple Combinations of Lineage-Determining Transcription Factors Prime cis-Regulatory Elements Required for Macrophage and B Cell Identities. Mol. Cell 38, 576–589.

Jha, B.S., Rao, M., Malik, N., 2015. Motor neuron differentiation from pluripotent stem cells and other intermediate proliferative precursors that can be discriminated by lineage specific reporters. Stem Cell Rev. 11, 194–204.

Keene, J.D., Komisarow, J.M., Friedersdorf, M.B., 2006. RIP-Chip: the isolation and identification of mRNAs, microRNAs and protein components of ribonucleoprotein complexes from cell extracts. Nat. Protoc. 1, 302–7.

Lauria, F., Bernabò, P., Tebaldi, T., Joan, E., Groen, N., Perenthaler, E., Maniscalco, F., Rossi, A., Donzel, D., Clamer, M., Marchioretto, M., Omersa, N., Orri, J., Serra, M.D., Anderluh, G., Quattrone, A., Inga, A., Gillingwater, T.H., Viero, G., 2020. of transcripts related to spinal muscular atrophy. Nat. Cell Biol. 22.

Panda, A.C., Martindale, J.L., Gorospe, M., 2017. Polysome Fractionation to Analyze mRNA Distribution Profiles Amaresh. Bio Protoc. 7.

Skowronska-Krawczyk, D., Ma, Q., Schwartz, M., Scully, K., Li, W., Liu, Z., Taylor, H., Tollkuhn, J., Ohgi, K.A.,

Notani, D., Kohwi, Y., Kohwi-Shigematsu, T., Rosenfeld, M.G., 2014. Required enhancer-matrin-3 network interactions for a homeodomain transcription program. Nature 514, 257–261.

Supek, F., Bošnjak, M., Škunca, N., Šmuc, T., 2011. Revigo summarizes and visualizes long lists of gene ontology terms. PLoS One 6.

Tebaldi, T., Re, A., Viero, G., Pegoretti, I., Passerini, A., Blanzieri, E., Quattrone, A., 2012. Widespread uncoupling between transcriptome and translatome variations after a stimulus in mammalian cells. BMC Genomics.

Thongon, N., Castiglioni, I., Zucal, C., Latorre, E., D'Agostino, V., Bauer, I., Pancher, M., Ballestrero, A., Feldmann, G., Nencioni, A., Provenzani, A., 2016. The GSK3β inhibitor BIS I reverts YAP-dependent EMT signature in PDAC cell lines by decreasing SMADs expression level. Oncotarget 7.

von Mering, C., Huynen, M., Jaeggi, D., Schmidt, S., Bork, P., Snel, B., 2003. STRING: A database of predicted functional associations between proteins. Nucleic Acids Res.